Journal of South American Earth Sciences 97 (2020) 102399

Contents lists available at ScienceDirect

Journal of South American Earth Sciences

journal homepage: www.elsevier.com/locate/jsames

Strontium Isotope Stratigraphy and the thermophilic fossil fauna from the middle Miocene of the East Pisco Basin (Peru)

Giulia Bosio[a,b,*], Elisa Malinverno[b], Alberto Collareta[a], Claudio Di Celma[c], Anna Gioncada[a], Mariano Parente[d], Fabrizio Berra[e], Felix G. Marx[f,g,h], Agostina Vertino[b,i], Mario Urbina[j], Giovanni Bianucci[a]

[a] Dipartimento di Scienze Della Terra, Università di Pisa, 56126, Pisa, Italy
[b] Dipartimento di Scienze Dell'Ambiente e Della Terra, Università Degli Studi di Milano-Bicocca, 20126, Milano, Italy
[c] Scuola di Scienze e Tecnologie, Università di Camerino, 62032, Camerino, Italy
[d] Dipartimento di Scienze Della Terra, Dell'Ambiente e Delle Risorse, Università Degli Studi di Napoli Federico II, 80126, Napoli, Italy
[e] Dipartimento di Scienze Della Terra "Ardito Desio", Università di Milano, 20126, Milano, Italy
[f] Directorate of Earth and History of Life, Royal Belgian Institute of Natural Sciences, 1000, Brussels, Belgium
[g] School of Biological Sciences, Monash University, VIC 3800, Clayton, Victoria, Australia
[h] Palaeontology, Museums Victoria, VIC 3053, Melbourne, Victoria, Australia
[i] Department of Geology, Renard Centre of Marine Geology, Universiteit Gent, 9000, Ghent, Belgium
[j] Departamento de Paleontología de Vertebrados, Museo de Historia Natural, Universidad Nacional Mayor de San Marcos, Lima 1, Peru

ARTICLE INFO

Keywords:
$^{87}Sr/^{86}Sr$ stratigraphy
Diagenesis evaluation
Miocene
Mollusks
Shark teeth
Cetaceans

New age estimates obtained via Strontium Isotope ($^{87}Sr/^{86}Sr$) Stratigraphy and new paleoclimatic data are here presented for the Miocene Chilcatay and Pisco formations exposed in the East Pisco Basin, an Andean forearc basin of southern Peru, which is renowned worldwide for its exceptional content of fossil marine vertebrates. Mollusk and barnacle shells, carbonate nodules, and shark teeth were collected along three stratigraphic sections for applying Strontium Isotope Stratigraphy on both carbonates and phosphates. To avoid diagenetic biases, mollusk and barnacle shells were analyzed in detail by means of optical and scanning electron microscopy, cathodoluminescence, and inductively coupled plasma-optical emission spectrometry, whereas only the enameloid from the best-preserved shark teeth was sampled. The obtained $^{87}Sr/^{86}Sr$ ages confirm a late early Miocene (Burdigalian) age for the Chilcatay strata, and reveal middle Miocene (Langhian to Serravallian) ages for the lower Pisco unit (i.e., the P0 sequence) – a result that matches the relatively archaic aspect of its cetacean fossil assemblage. New and literature data about the fossil assemblage of the lower Pisco beds highlight the presence of several thermophilic invertebrates and vertebrates, thus suggesting a warm-water, tropical paleoenvironment for this middle Miocene sequence. Such a paleoenvironmental scenario recalls the warm conditions associated with the Chilcatay Formation, rather than the cooler setting inferred for the remainder of the Pisco Formation (i.e., the P1 and P2 sequences). This pattern likely reflects the late Miocene trend of global cooling, as well as a middle to early late Miocene strengthening of the Humboldt Current.

1. Introduction

The $^{87}Sr/^{86}Sr$ ratio of strontium (Sr) in the global ocean has varied through the geological time (McArthur, 1994; McArthur et al., 2012). At the same time, the world's seas are homogeneous with respect to $^{87}Sr/^{86}Sr$ ratio, and this is assumed for any geologic time (McArthur et al., 2012). Therefore, Sr isotope composition can be used for dating marine minerals and correlating marine sedimentary successions worldwide (Faure and Mensing, 2005). Application of Strontium Isotope Stratigraphy (hereinafter: SIS) requires measurement of the Sr isotope ratio of minerals that precipitated from seawater and have not undergone diagenetic alteration of their original $^{87}Sr/^{86}Sr$ value (McArthur et al., 2012). Some intervals of geological time, such as the Miocene, are particularly favorable for the implementation of SIS because they display high rates of change of the $^{87}Sr/^{86}Sr$ value and a narrow error band on the empirically defined reference curve (McArthur et al., 2012), which allow for high-resolution age estimates.

The Miocene Chilcatay and Pisco formations exposed in the East

* Corresponding author. Dipartimento di Scienze Della Terra, Università di Pisa, 56126, Pisa, Italy.
E-mail address: giulia.bosio.giulia@gmail.com (G. Bosio).

https://doi.org/10.1016/j.jsames.2019.102399
Received 3 August 2019; Received in revised form 13 October 2019; Accepted 21 October 2019
Available online 25 October 2019
0895-9811/

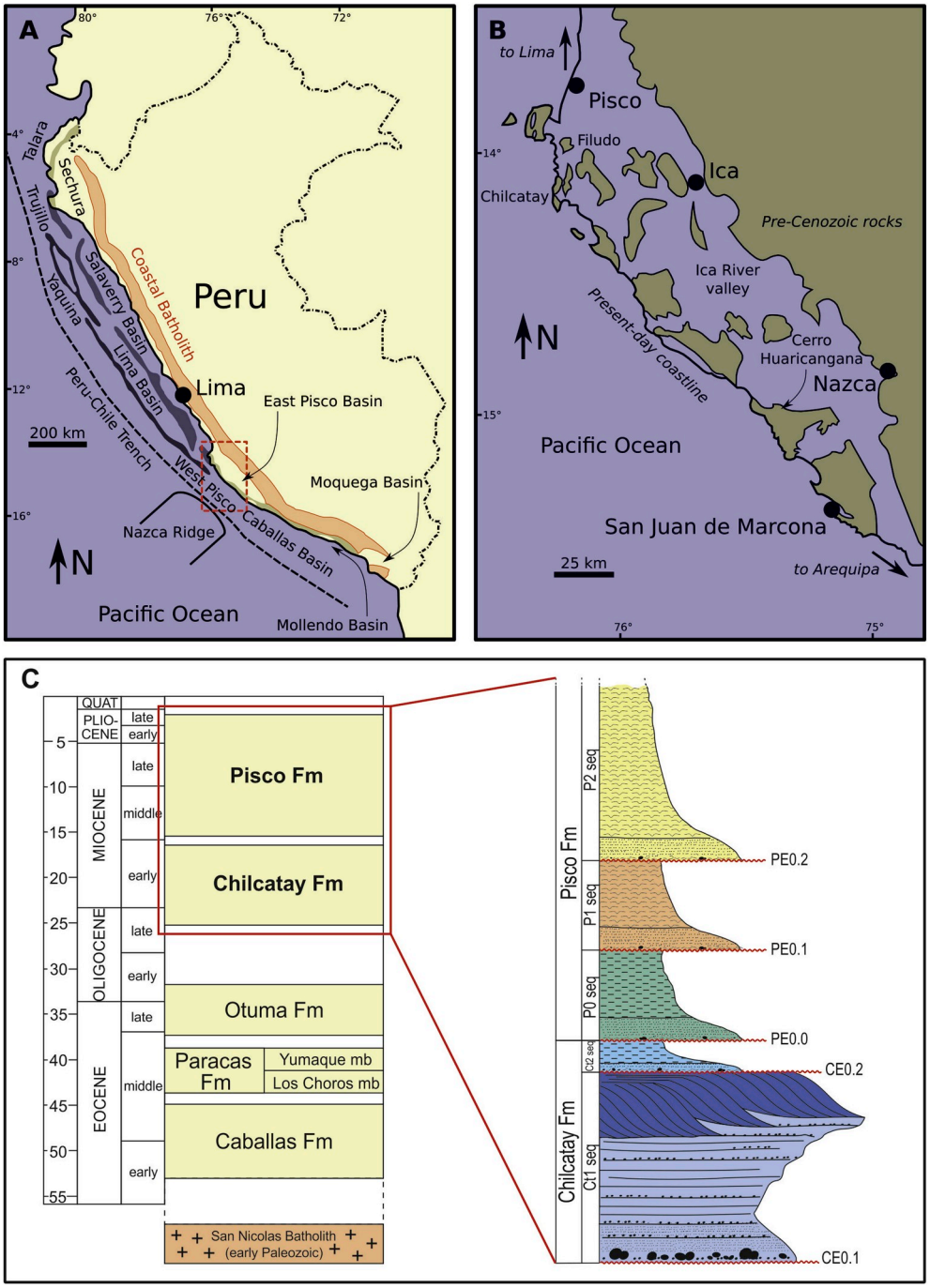

Fig. 1. A. Map of the major Cenozoic sedimentary basins along the Peruvian coast. Major structural highs are the Coastal Batholith, the Outer Shelf High and the Upper Slope Ridge. Redrawn and modified from Travis et al. (1974) and Thornburg and Kulm (1981). **B.** Paleoenvironmental reconstruction of the Peruvian coast during the Miocene. Islands are hypothesized on the basis of the distribution of the pre-Cenozoic rocks. Redrawn and modified from DeVries and Schrader (1997). **C.** Schematic stratigraphic column of the East Pisco Basin (from the Eocene to the present-day, ages are in Ma) with a close-up of the Chilcatay and Pisco formations and their internal subdivisions in sequences. Modified after Coletti et al. (2019) and Landini et al. (2019).

Pisco Basin of southern Peru are renowned for their exceptional fossil assemblage, comprising cetaceans, seals, sharks, rays, crocodiles, turtles, seabirds, and bony fishes (e.g., Bianucci et al., 2015, 2016a, 2016b, 2016c, 2018a, 2018b; Lambert et al., 2014, 2015b, 2017a, 2017b, 2018; Landini et al., 2017a, Landini et al., 2017, 2019; Marx et al., 2017a, 2017b; Gioncada et al., 2018b) as well as marine invertebrates (e.g., DeVries and Frassinetti, 2003; DeVries et al., 2006; DeVries, 2016; Coletti et al., 2018, 2019, in press; Collareta et al., 2019). In particular, the fossil record of the Pisco Formation is outstanding in terms of both abundance and preservation state of the vertebrate remains. Examples of exceptionally preserved fossil vertebrate specimens from the Pisco strata exposed in the East Pisco Basin include phosphatized baleen bristles and plates of mysticete whales (Brand et al., 2004; Esperante et al., 2008; Gioncada et al., 2016; Marx et al., 2017a), stomach contents and regurgitations of mysticete and odontocete cetaceans (Collareta et al., 2015; Lambert et al., 2015a), and phosphatized skeletons of cartilaginous fishes such as sharks (Collareta et al., 2017).

For interpreting this extraordinary paleontological heritage and enhancing its scientific significance, its placement in a robust stratigraphic context supported by reliable age estimates is crucial. Recent work established a chronostratigraphic framework based on ^{39}Ar–^{40}Ar dating, tephrostratigraphy and biostratigraphy, which dates the Chilcatay Formation to the early Miocene and the upper sequences of the Pisco Formation to the late Miocene, respectively (Di Celma et al., 2017, 2018a, b; Gariboldi et al., 2017; Bosio et al., 2019a, Bosio et al., 2019b). The seemingly large temporal gap between these two units is striking, but is almost certainly an overestimate caused by a lack of datable ash layers and microfossils from the lowermost portion of the Pisco Formation (the P0 sequence). Previous studies remarked on the

significantly archaic aspect of the cetacean fauna from this layer (Di Celma et al., 2017; Marx et al., 2017b), but were unable to draw definitive conclusions as to its age. The peculiar faunal changes that characterize this sequence (Di Celma et al., 2017) make the dating of these strata an issue of prime importance for the ongoing paleontological studies on the Miocene fossil content of the East Pisco Basin.

Here, we present the first attempt to date the lower Pisco beds by means of SIS. Mollusk (i.e., ostreids and pectinids) and barnacle shells, diagenetic cements, bulk cemented sediment, and shark teeth were collected to apply this method to both carbonates and phosphates. Several samples from the well dated Ct1 sequence of the Chilcatay Formation were dated for checking the reliability of the Sr isotope ratio results in the study areas. The preservation state of the invertebrate remains was preliminary addressed via petrographic, morphological, chemical, and cathodoluminescence analyses in order to quantify the extent of diagenetic alteration and to assess whether the shells were structurally and chemically pristine. Sr isotope ratios were elaborated with the LOWESS Table 5 made for the GTS2012 timescale (McArthur et al., 2012) and SIS ages were obtained.

Furthermore, we investigated the faunal assemblages of P0 for reconstructing the paleoenvironmental and paleoclimatic significance of this sequence in the light of our age estimates. Having been deposited in a key time interval that saw first-order changes of the climate and oceanographic system at both the global scale (e.g., the Middle Miocene Climatic Optimum and the Middle Miocene Climatic Transition) and the regional scale (e.g., the emergence of the modern upwelling regime along the Pacific margin of South America), the P0 beds and their newly dated fossil content represent indeed crucial elements for reconstructing the mode and tempo of the major Miocene environmental shift episodes off the coast of Peru – the current location of the outstandingly productive Humboldt Current (Penven et al., 2005).

2. Geological and paleontological framework

The East Pisco Basin is one of the elongated extensional/pull-apart sedimentary basins along the composite transform-convergent Peruvian margin (e.g., Thornburg and Kulm, 1981; Kulm et al., 1982; Dunbar et al., 1990; León et al., 2008; Zúñiga-Rivero et al., 2010) (Fig. 1A). Its emersion and subaerial exposure is due to the subduction of the nearby Nazca Ridge, a region of topographically high oceanic crust impinging on the Peru-Chile trench (Pilger, 1981; Hsu, 1992; Macharé and Ortlieb, 1992; Hampel, 2002). The basin fill comprises, in stratigraphic order, the Eocene Caballas and Paracas formations, the upper Eocene to lower Oligocene Otuma Formation, and the largely Miocene Chilcatay and Pisco formations (Dunbar et al., 1990; DeVries, 1998,2017; DeVries et al., 2017; DeVries and Jud, 2018) (Fig. 1C). These units are bounded by regionally extensive unconformities and are also internally divided by less pronounced intraformational unconformities (DeVries, 1998; Di Celma et al., 2017, 2018a, b). As such, this succession can be subdivided using both a lithostratigraphic and an allostratigraphic approach (North American Commission on Stratigraphic Nomenclature [NACSN], 2005). In the present paper, we refer to the internal informal units as “sequences”.

During deposition of the Chilcatay and Pisco formations, the East Pisco Basin was a semi-enclosed, shallow-marine bay, structured along a latitudinal depth gradient, and sheltered seawards by a longshore chain of crystalline basement islands (Fig. 1B) (Marocco and Muizon, 1988; DeVries and Jud, 2018; Bianucci et al., 2018).

The Chilcatay Formation was deposited during the late early Miocene, between 19 and 17 Ma (Burdigalian) (Di Celma et al., 2018b; Belia et al., 2019; Bosio et al., 2019b). It is composed of two distinct sequences, namely, Ct1 and Ct2 (Di Celma et al., 2018b, 2019) (Fig. 1C). At Ullujaya (14°34′59″S; 75°38′27″W) and Roca Negra (14°39′04″S; 75°38′54″W), two localities along the western side of the Ica River (Figs. 2A and 3A, B), the lower sequence (Ct1) of the Chilcatay Formation consists of massive sandstones and conglomerates with boulder-sized clasts at the bottom (*Ct1c* facies association), followed by medium-to fine-grained sandstones alternating with conglomerate beds (*Ct1a*), and clinobedded coarse-grained calcirudites at the top (*Ct1b*) (Di Celma et al., 2018b, 2019). These facies associations record deposition in the shoreface, offshore, and on a mixed siliciclastic-carbonate subaqueous delta, respectively (Di Celma et al., 2019), and suggest a semi-protected embayment associated with both a river mouth and the open ocean (Bianucci et al., 2018). The invertebrate fossil assemblage of the Chilcatay strata exposed at the study sites comprises mollusks, barnacles, serpulids and echinids (Di Celma et al., 2018b, 2019). Bivalves are represented by ostreids, pectinids and venerids. Barnacles mainly belong to three taxa, with *Austromegabalanus carrioli* being the most abundant (Coletti et al., 2018, in press; Collareta et al., 2019). The vertebrate fossil assemblage is dominated by toothed cetaceans (Odontoceti), including the peculiar longirostrine homodont species *Chilcacetus cavirhinus* and the archaic heterodont one *Inticetus vertizi*, as well as several other taxa of eurhinodelphinids, kentriodontids, platanistoids and physeteroids (Bianucci et al., 2015, Bianucci et al., 2018; Lambert et al., 2014, 2015b, 2018; Di Celma et al., 2018b, 2019). In addition, there are sea turtles (large-sized indeterminate dermochelyids), bony fishes and elasmobranchs, with abundant juvenile teeth of the copper shark *Carcharhinus brachyurus* and the extinct lamniform *Cosmopolitodus hastalis*. Overall, the fossil assemblage hints at a coastal community dominated by warm-water mesopredators (Bianucci et al., 2018).

The Pisco Formation is composed of three fining-upward sequences, designated P0, P1, and P2 from oldest to youngest, which are divided by three unconformities, named PE0.0, PE0.1, PE0.2, respectively (Fig. 1C). Each unit, representing a transgressive cycle, recorded deposition in shoreface (sandstones) and in offshore (siltstones/diatomaceous siltstones) settings. The time of deposition of the P1 and P2 sequences is late Miocene and is well-constrained between 9.5 Ma and 8.6 Ma, and between 8.4 and 6.7 Ma, respectively (Gariboldi et al., 2017; Bosio et al., 2019, Bosio et al., 2019b). Due to the lack of tephra layers and microfossils, the depositional age of the lower unit, P0, is to date very poorly constrained between 18 and 9.5 Ma (Di Celma et al., 2017; Bosio et al., 2019b). Note, however, that DeVries and Jud (2018) previously proposed an early–middle Miocene age for the lower portion of the Pisco Formation (including P0), based on a series of diatom samples analyzed by H. Schrader in the 1980s. The P0 strata of the Pisco Formation reach their maximum thickness (about 40 m) at the locality of Cerro Submarino (14°34′38″S; 75°39′51″W) (Fig. 3D). This unit is mostly composed of fine- to very coarse-grained, cross-stratified, fossil-rich sandstones, suggesting a very nearshore environment. The fossil invertebrate assemblage of P0 is dominated by mollusks, with barnacles being less common. Mollusks are mostly represented by bivalves and primarily include *Chionopsis* spp. and *Dosinia ponderosa*, but *Miltha* cf. *vidali* and ostreids are also present (Di Celma et al., 2017). Vertebrates are abundant, but less studied than those from the underlying Chilcatay strata. Baleen whales (Cetacea: Mysticeti) dominate the assemblage and are represented by i) a large-sized stem balaenopteroid, *Pelocetus* sp. (Bianucci et al., 2019); ii) the archaic cetotheriid *Tiucetus rosae*, previously described from the southeastern locality of Santa Rosa (Marx et al., 2017b); and iii) a third form, previously identified as a cetotheriid (Di Celma et al., 2017), but here more conservatively reinterpreted as an indeterminate mysticete more closely related to extant rorquals and gray whales than to extant right whales. Toothed whales include at least one physeteroid and two kentriodontid-like delphinoids. In addition, there are fragmentary fossils of chelonioid turtles and longirostrine crocodilians, and a single bird specimen identified as an indeterminate pelagornithid (Di Celma et al., 2017). Shark and ray teeth are relatively common and include, among others, *Carcharocles megalodon*, *Cosmopolitodus hastalis*, *Isurus oxyrinchus*, and myliobatids (eagle rays) (Di Celma et al., 2017).

Fig. 2. Satellite image and position of the localities of Cerro Submarino (14°34′38″S; 75°39′51″W), Ullujaya (14°34′59″S; 75°38′27″W), and Roca Negra (14°39′04″S; 75°38′54″W) along the western side of the Ica River (Ica Desert). Based on a Google Earth image (© 2019 Maxar Technologies).

3. Material and methods

3.1. Study area and sample collection

The study area is settled in the Ica Desert, at the localities of Roca Negra (sampling site: 14°39′04″S; 75°38′54″W) and Ullujaya (sampling site: 14°34′59″S; 75°38′27″W), where the Chilcatay Formation crops out (Di Celma et al., 2018b, 2019; Bianucci et al., 2018), and Cerro Submarino (sampling site: 14°34′38″S; 75°39′51″W), where P0 displays its maximum thickness (40 m) (Figs. 2 and 3).

From 2015 and during five successive field campaigns, the Chilcatay and Pisco outcrops at the localities of Roca Negra, Ullujaya, and Cerro Submarino were investigated in detail for fossil vertebrates and macroinvertebrates by means of systematic surface prospecting. Preliminary identifications of the surveyed fossil specimens were made in the field. A few highly significant specimens, including representatives of the thermophilic taxa reported herein, were collected and deposited in the Museo de Historia Natural de la Universidad Nacional Mayor de San Marcos (MUSM) in Lima for preparation and study.

Samples collected for applying the SIS were carbonates (invertebrate shells, diagenetic cements) and phosphates (shark teeth). For the Sr isotope analyses, shark tooth fluorapatite and low-Mg calcite shells were preferred, as low-Mg calcite is more stable during diagenesis and less soluble than other carbonates (Brand, 1991; Steuber, 2003). Mollusks (i.e., ostreids and pectinids) and barnacles, shark teeth, and bulk and cement samples were collected along the measured section of the well-dated Chilcatay Formation at Roca Negra and Ullujaya, as well as from the undated P0 deposits at Cerro Submarino (Figs. 2 and 3). Different horizons were selected at each locality (Fig. 3, C) and, for each level, several carbonate shells were sampled, usually from different organisms (e.g., oysters, pectinids, and barnacles). Some bulk and cement samples were also analyzed for better understanding the diagenetic path and its effects on $^{87}Sr/^{86}Sr$ values.

3.2. Optical microscopy (OM), scanning electron microscopy (SEM), and cathodoluminescence

Diagenetic processes or weathering could modify the pristine $^{87}Sr/^{86}Sr$ ratio of carbonate and phosphate marine minerals, providing wrong ages of mineral formation (Scasso et al., 2001; Brand et al., 2012; Ullmann and Korte, 2015). Therefore, their identification is critical for evaluating the reliability of the $^{87}Sr/^{86}Sr$ ratio, which is suitable for SIS only when post-depositional alterations can be excluded. With the aim of evaluating the impacts of diagenesis and weathering on shells, mollusk and barnacle samples from both the Chilcatay and Pisco formations have been prepared for realizing thin sections. Petrographic analyses of polished thin sections were carried out through Leica and Olympus optical microscopes. A SEM-EDS Tescan VEGA TS Univac 5136XM was used at the Department of Earth and Environmental Sciences of the Università degli Studi di Milano-Bicocca for petrographic and morphological observations, as well as for checking evidence of dissolution in the structure of the selected shells. Cathodoluminescence was performed using a CITL Optical Cathodoluminoscope at the Department of Earth Science "Ardito Desio" of the Università degli Studi di Milano, operated at about 14 kV accelerating voltage and 0.5 mA gun current intensity. Cathodoluminescence observations permitted the identification of different carbonate generations, as well as of recrystallized portions of the shells (Barbin, 2013; Ullmann and Korte, 2015).

Pristine shells were chosen for the age calculation, whereas shells showing a recrystallized and/or dissolved texture under both the optical and the electron microscope, and a high luminescence under the cathodoluminoscope were discarded. Some recrystallized materials were also selected for $^{87}Sr/^{86}Sr$ analyses, for understanding how diagenesis changed the Sr ratio (i.e., diagenesis path) (Steuber, 2003). Regarding shark teeth, samples were taken from the outer enameloid layer (Enax et al., 2014), avoiding dentine, which is generally more porous and susceptible to diagenetic alteration than enameloid (Becker et al., 2008). Sr isotope measurement on the enameloid portion of shark teeth has proven to provide reliable age estimates (Becker et al., 2008; Harrel et al., 2016).

After the preliminary analyses, fifteen samples were selected from the Ct1 sequence of the Chilcatay Formation, whereas eight samples were selected from the P0 sequence of the Pisco Formation (Table 1).

3.3. Compositional and strontium isotope analyses

After microscopic investigations, the selected pristine mollusk shells and well-preserved barnacle sheaths were carefully cleaned through an ultrasonic bath in distilled water. They were bored with a Dremel micro-drill to obtain shell powder from the diagenetically unaltered portion. After an ultrasonic bath in distilled water, the selected shark teeth were also scraped with the micro-drill and powder of their unaltered, non-porous enameloid was collected. About 10–50 mg of each

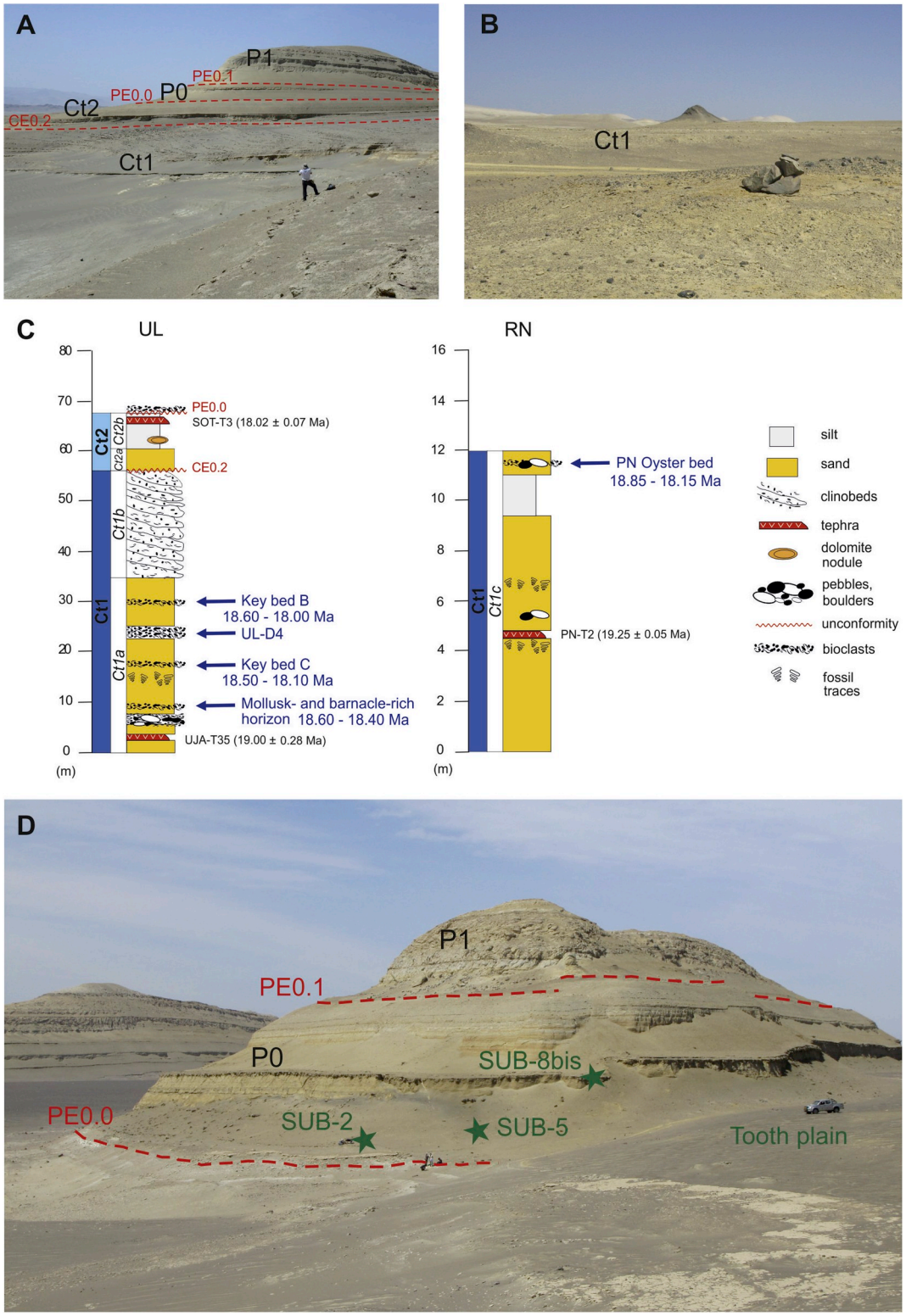

Fig. 3. A. Field photo of the Chilcatay and Pisco strata at the locality of Ullujaya. Unconformities are traced in red. **B.** Field photo of the Chilcatay basal strata at the locality of Roca Negra. **C.** Schematic stratigraphic sections measured at the Chilcatay outcrops of Ullujaya (UL) and Roca Negra (RN) that show the stratigraphic position of i) the investigated beds and their $^{87}Sr/^{86}Sr$ ages and ii) the ash layers with the previous $^{39}Ar–^{40}Ar$ ages obtained by Bosio et al., 2019b. **D.** Field photo at Cerro Submarino, with the location of the sampled beds (green stars) collected from the P0 sequence. The PE0.0 and PE0.1 unconformities are traced in red. (For interpretation of the references to colour in this figure legend, the reader is referred to the Web version of this article.)

sample were collected for inductively coupled plasma-optical emission spectroscopy (ICP-OES) and $^{87}Sr/^{86}Sr$ analyses, taking care to avoid contaminations.

ICP-OES and $^{87}Sr/^{86}Sr$ analyses were made at the Institute für Geologie, Mineralogie und Geophysik of the Ruhr-Universität of Bochum. ICP-OES analyses were made with a Thermo Fisher Scientific iCAP 6500 DUO spectrometer for analyzing the concentrations of Sr, Ca (calcium), Mg (magnesium), Fe (iron), and Mn (manganese).

Table 1
Sample list and description, with locality and stratigraphic data, reporting $^{87}Sr/^{86}Sr$ measured values and standard deviation, with $^{87}Sr/^{86}Sr$ values corrected for the difference between the USGS EN-1 value used for the compilation of the reference curve (McArthur et al., 2012) and the USGS EN-1 Bochum mean value.

Formation	Sequence	Locality	Stratigraphic level	Samples	Description	Measured $^{87}Sr/^{86}Sr$	± $2s_{mean}$	Corrected $^{87}Sr/^{86}Sr$
Pisco Fm	P0	Cerro Submarino	SUB-8bis	SUB-8bis1	Barnacle sheath	0.708811	0.000005	0.708827
				SUB-8bis2	Bulk cemented sediment	0.708273	0.000005	0.708289
				SUB-8bis3	Recrystallized bivalve shell	0.708650	0.000005	0.708666
			SUB-5	SUB-5	Ostreidae specimen	0.708804	0.000005	0.708820
			SUB-2	SUB-2	Calcite nodule	0.708557	0.000005	0.708573
			Tooth plain	Tooth 1	Shark tooth: *Cosmopolitodus hastalis*	0.708803	0.000005	0.708819
				Tooth 2	Shark tooth: *Cosmopolitodus hastalis*	0.708778	0.000005	0.708794
				Tooth 3	Shark tooth: *Isurus oxyrinchus*	0.708784	0.000005	0.708800
Chilcatay Fm	Ct1	Ullujaya	Key bed B	UJA-2a	Ostreidae specimen	0.708541	0.000005	0.708557
				UJA-2b	Ostreidae specimen	0.708523	0.000005	0.708539
			UL-D4	UL-D4a	Ostreidae specimen	0.708506	0.000004	0.708522
				UL-D4b	Barnacle sheath	0.708617	0.000005	0.708633
				UL-D4c	Bulk cemented sediment	0.708444	0.000005	0.708460
			Key bed C	UJA-LIVC1	Ostreidae specimen	0.708535	0.000005	0.708551
				UJA-LIVC2	Bulk cemented sediment	0.708340	0.000005	0.708356
				UJA-LIVC3	Ostreidae specimen	0.708542	0.000005	0.708558
				UJA-LIVC4	Barnacle sheath	0.708521	0.000005	0.708537
			Mollusc- and barnacle-rich horizon	UL-LIVa	Barnacle sheath	0.708516	0.000005	0.708532
				UL-LIVb	Pectinidae specimens	0.708512	0.000005	0.708528
				UL-LIVd	Pectinidae specimen	0.708514	0.000005	0.708530
		Roca Negra	PN Oyster bed	PN-OST	Ostreidae specimen	0.708498	0.000005	0.708514
				PN-GIO1	Ostreidae specimen	0.708513	0.000007	0.708529
				PN-GIO2	Ostreidae specimen	0.708536	0.000005	0.708552

$^{87}Sr/^{86}Sr$ ratios were determined with a TIMS Finnigan MAT 262 solid source mass spectrometer with seven collectors, using a dynamic (peak-hopping) mode of measurement. The cut-off limit for a strontium run was an error of $\pm 2\sigma \leq 5 \times 10^{-6}$ for the $^{87}Sr/^{86}Sr$ ratio, with 100–200 ratios per run (typical duration: 110 ratios, lasting 2 h 15 min, plus the filament heating time). Two standards – NIST NBS 987 and USGS EN-1 – were used to calibrate the analysis. NIST NBS 987 was loaded directly onto the filament, to confirm the stability of the mass spectrometer. USGS EN-1, a powder derived from a modern *Tridacna* shell, underwent the same procedure as the other carbonate samples, to ensure the reproducibility of the entire analytical process. Thirty-four analyses of NIST NBS 987 resulted in a mean of 0.710240 ± 0.000023 (2σ), while 24 analyses of USGS EN-1 yielded 0.709153 ± 0.000019 (2σ). No Rb (rubidium) correction was applied, but Rb was nonetheless monitored during the entire run. When Rb levels exceeded the detection limit, the result was discarded and the measurement repeated.

The results of the $^{87}Sr/^{86}Sr$ analyses were corrected for the difference between the USGS EN-1 value used for the compilation of the reference curve (McArthur et al., 2012) and the USGS EN-1 Bochum mean value, and then converted into ages using the LOWESS Table 5, which is tied to the GTS2012 timescale (McArthur et al., 2012). The latter is still incomplete, therefore the results were rounded off to the nearest value. Following the method described by Frijia et al. (2015), when more than one sample was analyzed for a single layer, a mean $^{87}Sr/^{86}Sr$ value was calculated. The uncertainty for each stratigraphic level was calculated as 2 s.e. (i.e., standard errors) from the standard deviation of the mean.

4. Results

4.1. Diagenesis evaluation

The Chilcatay and Pisco formations present notably divergent patterns of carbonate preservation. In the Chilcatay Formation, fossil invertebrates are well-preserved and retain their pristine calcitic shells. By contrast, in the Pisco Formation, calcitic shells are only present in the P0 sequence, where examples of calcite recrystallization also occur, but not in P1 and P2, where mollusks are only preserved as casts (Di Celma et al., 2017). For these reasons, SIS could only be applied in the Ct1 and P0 sequences, once some caveats have been taken into account, such as in-depth petrographic and chemical analyses of the samples.

At the macroscale, all of the bivalves selected for Sr analyses from both the units appear well-preserved and composed of calcite. The oysters (Fig. 4A) are usually incided by bioerosional marks, such as attachment traces by sponges and/or drill holes due to the predatory action of carnivorous gastropods; in several cases, they preserve layers of unaltered nacre. The pectinids (Fig. 4B) are also well-preserved, with small borings and some barnacle attachment traces (*Anellusichnus*; Santos et al., 2005). By contrast, the barnacles (Fig. 4C) generally display obvious signs of abrasion and lack their opercula; the best-preserved and less porous portion of the shell is often constituted by the sheath, the thickened upper part of the inner wall (see Fig. 4C). Shark teeth selected for Sr analyses are moderately-to well-preserved; although two shark teeth show a breakage surface in their root, they all have an intact thin layer of enameloid that surrounds the pulp cavity and covers the surface of the tooth crown (Fig. 4D).

Microscopically, the best-preserved pectinids and ostreids are characterized by foliated and prismatic calcite, respectively (Fig. 5A, C) (Cox et al., 1971). Both also have a low, homogeneous luminescence, suggesting little or no diagenesis (Fig. 5B, D). Nevertheless, some of the analyzed ostreids also have layers that are luminescent, documenting diagenetic modifications. Microborings filled by luminescent calcite or terrigenous sediments can be observed (Fig. 5C and D). These infills must be avoided during sampling for Sr isotope analyses, because they could add non-pristine Sr. As reported also by Crippa et al. (2016), fossil ostreids occasionally exhibit layers of sparry calcite replacing the pristine aragonitic layers (i.e., myostracum) or filling the chambers once permeated by organic matter (Fig. 5E and F). All those specimens that present similar features were discarded from the Sr analyses. Several oysters from the Ct1 and P0 sequences that exhibit a generally low luminescence have discrete luminescent layers that appear pristine and prismatic. For explaining this feature, which has also been documented in modern oysters, Barbin et al. (1991) and Barbin (2013) argued that luminescence may not be always a convincing indicator of

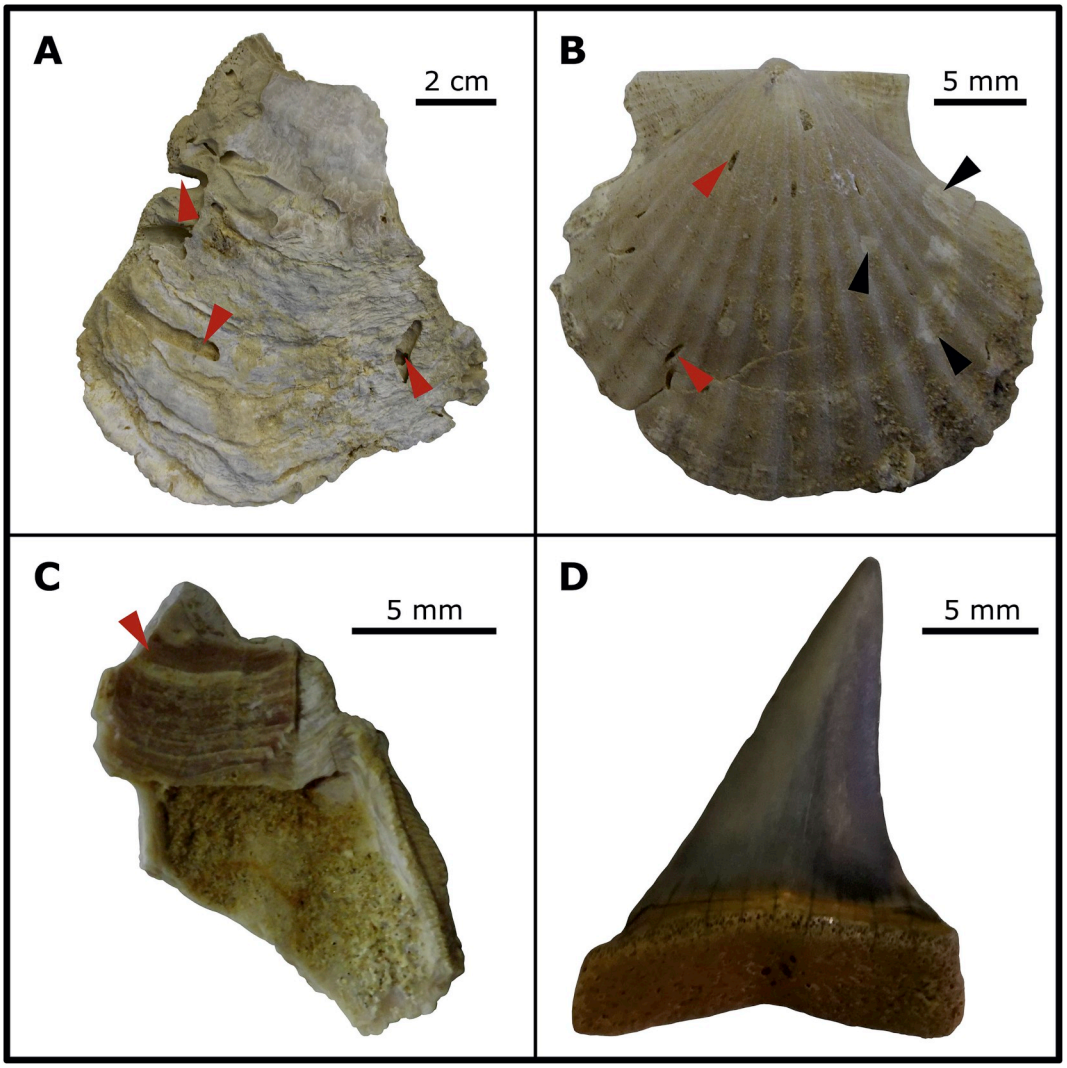

Fig. 4. A. Oyster shell from the PN Oyster level in the Ct1 sequence at Roca Negra. Note the bioerosional marks on the outer part of the shell pointed out by red arrows. **B.** Pectinid specimen from the mollusk- and barnacle-rich horizon in the Ct1 sequence at Ullujaya. Note the small bioerosional holes (red arrows) and the barnacle attachment scars (i.e., *Anellusichnus*) (black arrows). **C.** Barnacle plate from the Key bed C in the Ct1 sequence at Ullujaya. Note the lamellar sheath (i.e., the thickened upper part of the inner wall pointed out by the red arrow) from which the SIS samples were taken. **D.** Tooth of *Cosmopolitodus hastalis* from the P0 sequence at Cerro Submarino. (For interpretation of the references to colour in this figure legend, the reader is referred to the Web version of this article.)

diagenetic alteration for oysters, because the incorporation of Mn^{2+} by benthic organisms depends on various factors, such as growth rate, ontogeny, bathymetry, salinity, and redox conditions. To minimize the risk of diagenetic bias, we conservatively discarded all the ostreid samples with diffuse microborings, sparry calcite, or displaying high and/or heterogeneous luminescence. By contrast, the best-preserved barnacles are characterized by low luminescence throughout the less porous portion of the wall, but high luminescence charaterized the parietal tubes, which are normally filled with secondary calcite (Fig. 5G and H). We carefully avoided to contact the parietal tubes during sampling of the barnacle shells for the strontium analysis.

Secondary electron (SE) images confirmed the presence of alternating prismatic and sparry calcite layers in some ostreid specimens (Fig. 6A and B) that were hence discarded. Other specimens either retain a pristine prismatic layer (Fig. 6C) or show clear signs of alteration such as obliteration of the pristine prismatic texture (very irregular or dissolved) and widespread, pervasive holes (Fig. 6D). Again, specimens exhibiting obvious evidence of diagenesis were discarded.

ICP-OES analysis is useful for measuring the Fe, Mn, Mg, and Sr concentrations, which in turn can be informative in terms of diagenetic imprint on carbonates. Usually, the Fe and Mn contents of carbonates increase during the diagenetic processes; on the contrary, the Mg and Sr contents generally decrease during diagenesis (Brand and Veizer, 1980; McArthur, 1994; Steuber, 1999). Fixed or static limits for Fe, Mn and Sr content have been proposed by several authors to discriminate between pristine and altered biotic low-Mg calcite of fossil shells (see Ullmann and Korte, 2015 for a recent review). However, this approach totally ignores natural variation due to spatial and temporal differences (Brand et al., 2012; Ullmann and Korte, 2015). For this reason, following the approach of Brand et al. (2012), we evaluated separately each stratigraphic horizon, comparing the chemical composition of different coeval components (i.e. optically well-preserved shells, recrystallyzed shells, cemented bulk sediment enclosing or encrusting the shells) to select the best-preserved material. In Fig. 7A, the low Sr content of cement and bulk samples indicates a decrease in Sr during diagenesis, as reported by Frijia and Parente (2008) for diagenetically altered marine carbonates, coupled with a decrease of the $^{87}Sr/^{86}Sr$ value (see also the Supplementary Material). The latter trend is opposite to what is normally observed in diagenetically altered carbonates, when the interaction of the diagenetic fluids with siliciclastic rocks generally results in more radiogenic Sr isotope values (McArthur, 1994). The decrease of the Sr ratio in the diagenetically altered calcite of the studied

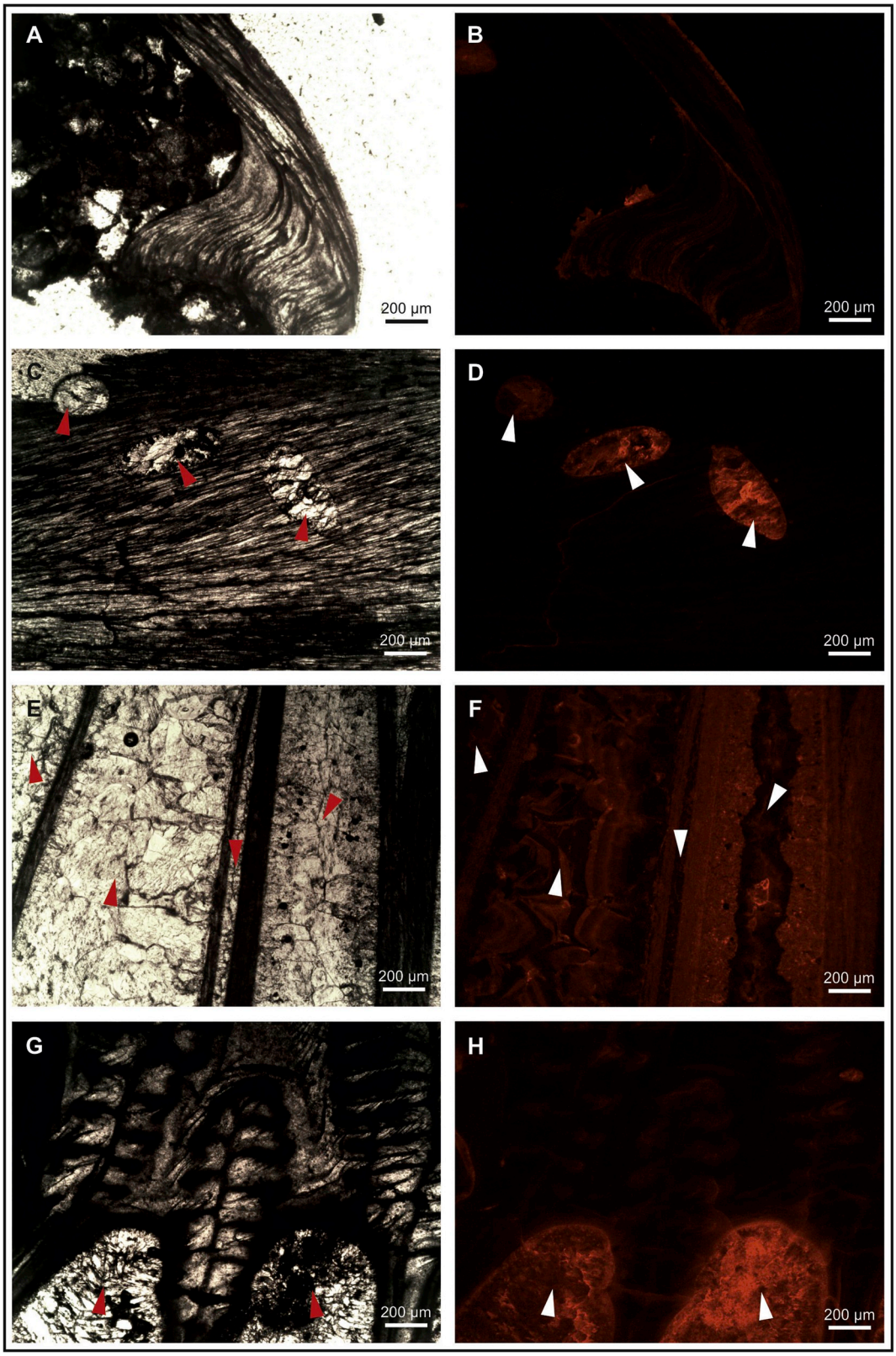

Fig. 5. Transmitted light and cathodoluminescence microscopical photos. **A, B.** Pectinid shell with a homogenous luminescence. **C, D.** Oyster prismatic layer with a low and homogeneous luminescence, punctuated by microborings with a high luminescence (red and white arrows). **E, F.** A poorly preserved oyster shell characterized by an alternation of high luminescent layers of sparry calcite (red and white arrows). **G, H.** Transverse thin section of a barnacle shell showing tree-like interlaminate figures and the parietal tubes filled by diagenetic calcite with a high luminescence pointed out by red and white arrows. (For interpretation of the references to colour in this figure legend, the reader is referred to the Web version of this article.)

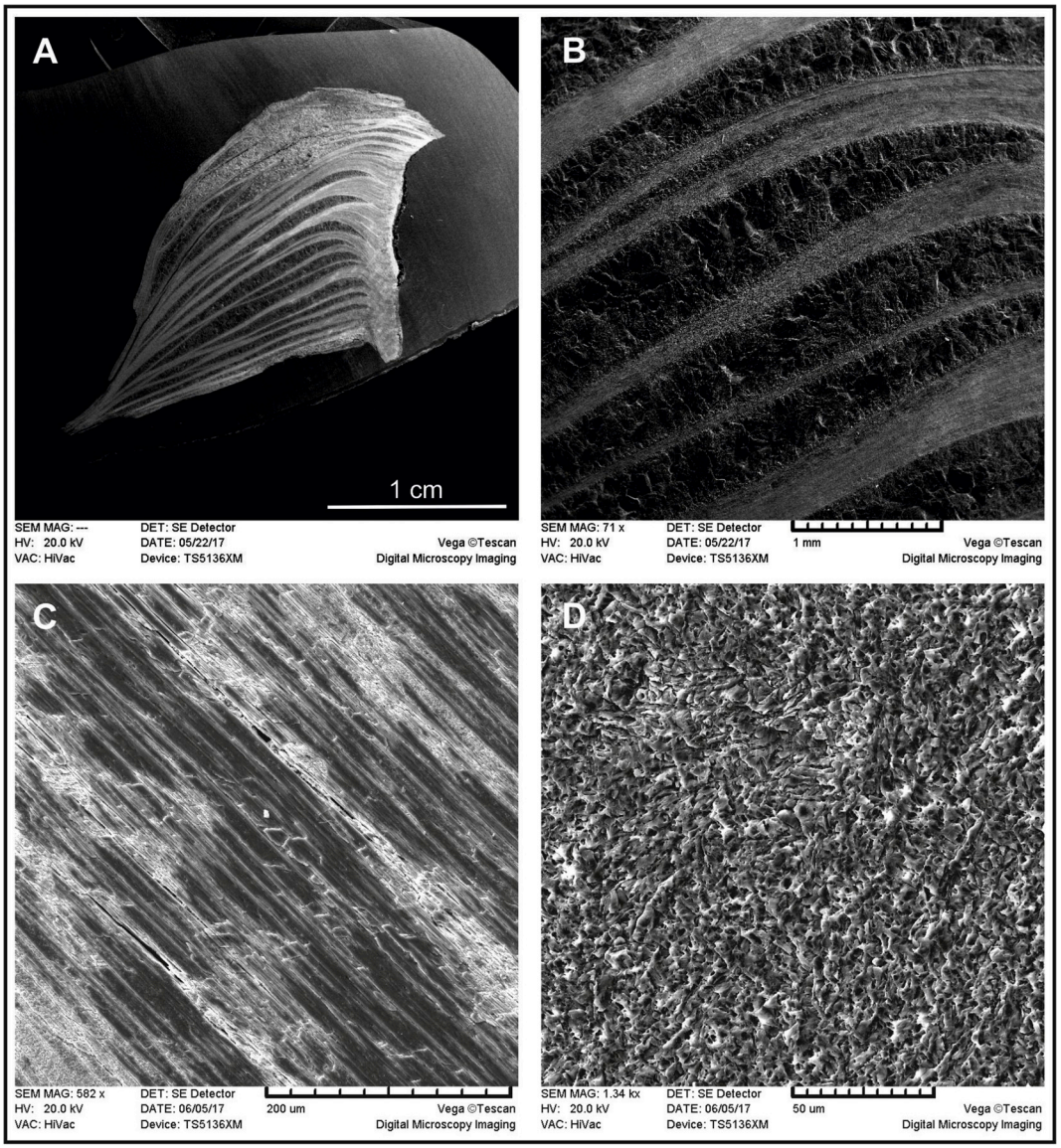

Fig. 6. A. SE (Secondary Electron) image of an oyster cross-section. Note the alternation of different layers. **B.** Close-up of the oyster shell depicted in panel A. Note the alternation of prismatic layers (light grey) and sparry calcite layers (dark grey). **C.** SE image of a well-preserved prismatic layer of an oyster. **D.** SE image of a poorly preserved oyster shell exhibiting dissolution features as obliteration of the pristine prismatic texture and widespread, pervasive holes.

successions can be due to pre-Miocene seawater-derived brine circulating within the sedimentary sequence, as reported by Gioncada et al. (2018a). This decrease of the Sr isotope ratio from pristine to diagenetic calcite confers older Sr ages to the diagenetically altered samples. The abundance of Fe and Mn in the diagenetic samples (see Fig. 7B, C, D) conforms to the expected pattern of increasing Fe and Mn concentration during diagenesis (see also the Supplementary Material). The above reconstruction of the diagenetic paths helps in assessing the preservation of each sample. Indeed, samples displaying the same degree of morphological preservation but higher concentrations of Sr and lower concentrations of Fe and Mn might be considered as retaining the pristine Sr isotope ratio of seawater.

4.2. Strontium Isotope Stratigraphy of the Ct1 sequence

After discarding all those shells that may have been affected by post-depositional modifications, fifteen samples from the Ct1 sequence of the Chilcatay Formation (Ullujaya and Roca Negra) were selected for $^{87}Sr/^{86}Sr$ analysis (Table 1). From each locality, Sr isotope analyses of different well-preserved shells yielded similar Sr isotope values (see Table 1 and Supplementary Material). The internal consistency of the Sr isotope ratios of different samples from the same stratigraphic level can be regarded as a strong argument supporting the preservation of the original seawater $^{87}Sr/^{86}Sr$ value (McArthur, 1994; Steuber, 2003).

At Roca Negra, we sampled three well-preserved oysters (PN-OST, PN-GIO1, PN-GIO2) from the *Ct1c* facies association. The three specimens came from a single bed (PN Oyster bed; Fig. 3C) close to the base of the formation, ca. seven meters above an ash layer (PN-T2) dated to 19.25 ± 0.05 Ma by Bosio et al., 2019b. Sr isotope analyses give similar $^{87}Sr/^{86}Sr$ results (Table 1) and the mean value gives a preferred age of 18.50 with a range of uncertainty spanning between 18.85 and 18.15 Ma (Table 2).

At Ullujaya, we sampled 12 specimens from the *Ct1a* facies association, between a basal ash layer (UJA-T35) dated to 19.00 ± 0.28 Ma by Bosio et al., 2019b and a second ash layer in the overlying *Ct2b* facies association (SOT-T3) dated to 18.02 ± 0.07 Ma by Di Celma et al. (2018b) (Fig. 3C).

Three samples – a barnacle sheath (UL-LIVa), composite sample of two pectinids (UL-LIVb), and a further, single pectinid (UL-LIVc) – were chosen from a layer 9 m above the base of the measured section

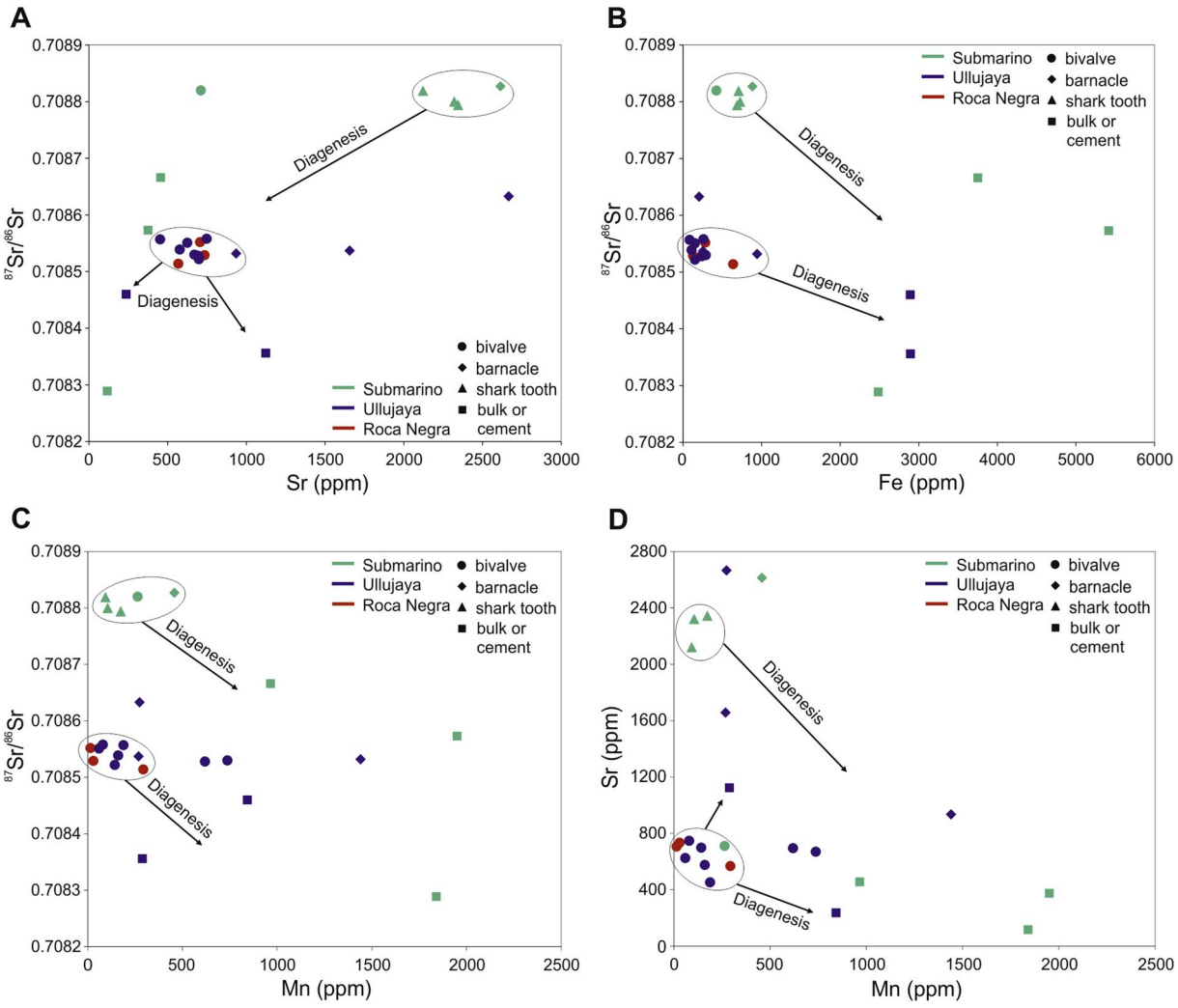

Fig. 7. Diagenetic path diagrams of the samples, showing the major trends of diagenetic alteration in multi-component plots. **A.** $^{87}Sr/^{86}Sr$ ratio vs Sr concentration. **B.** $^{87}Sr/^{86}Sr$ ratio vs Fe concentration. **C.** $^{87}Sr/^{86}Sr$ ratio vs Mn concentration. **D.** Sr vs Mn concentrations. Ellipses show the best-preserved samples. The arrows indicate the trends of diagenetic alteration.

(hereafter: abs), named "mollusk- and barnacle-rich horizon" by Collareta et al. (2019) (Fig. 3C). The mean value of the $^{87}Sr/^{86}Sr$ values gives again a preferred age of 18.50 Ma and an uncertainty that ranges from 18.60 to 18.40 Ma for this horizon (Table 2).

At 17 m abs, in occurrence of the key bed C (KbC of Di Celma et al., 2018b) (Fig. 3C), nacre layers of two well-preserved oysters were selected (UJA-LIVC1, UJA-LIVC3) together with a barnacle sheath (UJA-LIVC4) (Table 1). In addition, a sample of the cemented bulk sediment from the outer part of an oyster shell was also analyzed (UJA-LIVC2). Considering only the ages from the pristine shells, we obtained similar $^{87}Sr/^{86}Sr$ values and Burdigalian ages (see Tables 1 and 2). The bulk sample UJA-LIVC2 shows a lower value of $^{87}Sr/^{86}Sr$ ratio and gives older ages (i.e., 21.45–21.00 Ma), suggesting an ageing effect caused by diagenesis, as discussed above. The age range of the key bed C is thus comprised between 18.50 and 18.10 Ma, with a preferred age of 18.30 Ma (Table 2). The SIS age of this bed is apparently younger than that of the bed below (i.e., the mollusk- and barnacle-rich horizon), dated at ca. 18.50 Ma, although the two obtained age ranges are still largely overlapping.

Three samples were selected for the UL-D4 bed, a carbonate-rich horizon located 25 m abs (see Fig. 3C): UL-D4a, from prismatic layers of an oyster; UL-D4b, from a barnacle sheath; UL-D4c, the bulk sediment cemented within the same barnacle shell (Table 1). The bulk sample, UL-D4c, exhibits a relatively low $^{87}Sr/^{86}Sr$ value and, consequently, a relatively older age value (i.e., 19.60–19.20 Ma), indicating that diagenesis had an ageing effect on the shells also in this bed. The shell samples from the UL-D4 bed did not return consistent values of $^{87}Sr/^{86}Sr$ (see Table 1 and the Supplementary Material) and they were

Table 2
$^{87}Sr/^{86}Sr$ ages for the Ct1 and P0 sequences, calculated from the LOWESS Table 5 (McArthur et al., 2012).

	Stratigraphic level	*minus 2 s.e.*	$^{87}Sr/^{86}Sr$ mean value	*plus 2 s.e.*	Maximum age (Ma)	Preferred age (Ma)	Minimum age (Ma)
P0	Lower P0	0.708799	0.708812	0.708825	14.80	13.45	12.45
Ct1	Key bed B	0.708530	0.708548	0.708566	18.60	18.30	18.00
	Key bed C	0.708536	0.708549	0.708561	18.50	18.30	18.10
	Mollusk- and barnacle-rich horizon	0.708528	0.708530	0.708532	18.60	18.50	18.40
	PN Oyster bed	0.708510	0.708532	0.708554	18.85	18.50	18.15

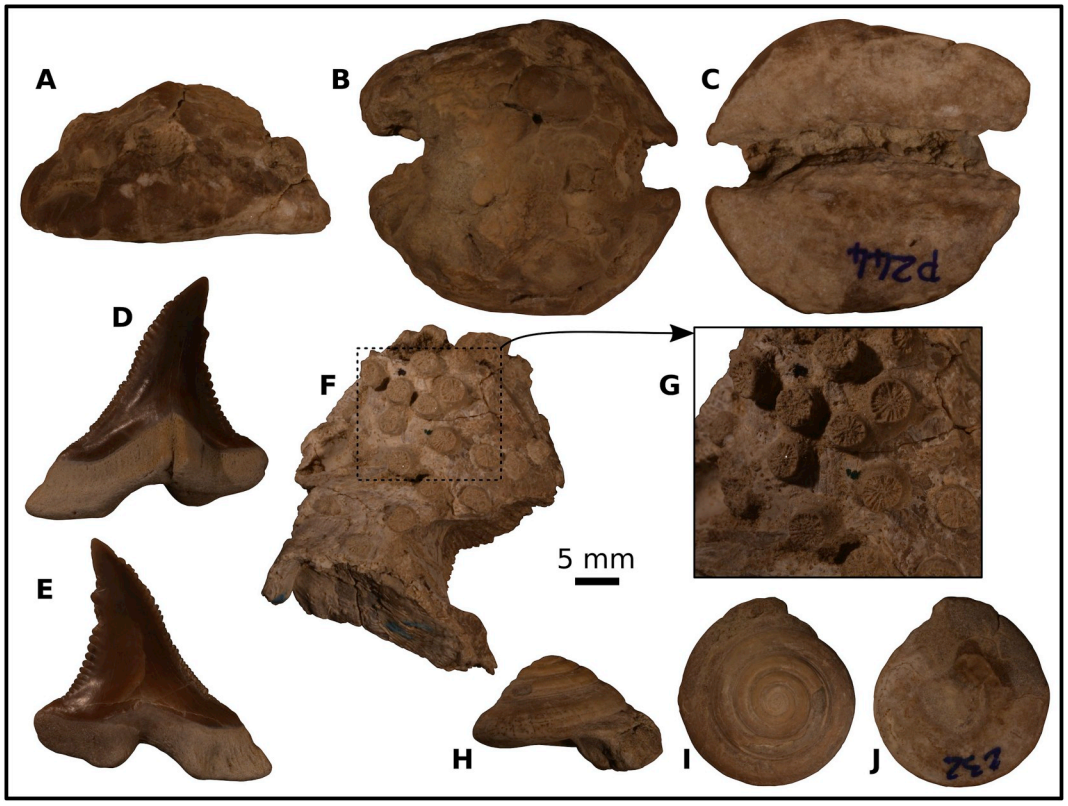

Fig. 8. Fossils of warm-water taxa from the P0 sequence. **A, B, C.** Cypraeid specimen in lateral (A), dorsal (B), and apertural (C) views. **D, E.** Tooth of *Hemipristis serra* in lingual (A) and labial (B) views. **F.** Rhizangiid corallites encrusting a cluster of barnacle shells. **G.** Close-up of the corallites depicted in panel F. **H, I, J.** Architectonicid specimen in lateral (H), dorsal (I), and ventral (J) views.

discarded from the age determination.

Finally, at 30 m abs, we took two samples (UJA-2a and UJA-2b) from different layers of a single oyster shell, collected from key bed B of Di Celma et al. (2018b) (Fig. 3C). The mean $^{87}Sr/^{86}Sr$ value provides a preferred age of 18.30 Ma for the key bed B, with a maximum age of 18.60 Ma and a minimum age of 18.00 Ma, in agreement with the levels dated below (Table 2).

The $^{87}Sr/^{86}Sr$ ages calculated for each bed give a Burdigalian age for the Ct1 sequence of the Chilcatay Formation. The time resolution of the SIS method is not sufficient to discriminate the age of these closely spaced horizons. However, the preferred ages of the sampled levels tend to be younger according to the stratigraphy.

4.3. Strontium Isotope Stratigraphy of the P0 sequence

Carbonates from the P0 sequence are poorly preserved, resulting in just five samples from a ~10 m-thick stratigraphic section located north of Cerro Submarino (Fig. 3D). Given the scarcity of suitable carbonate samples, we also collected samples from well-preserved shark teeth (phosphates). They show $^{87}Sr/^{86}Sr$ values that are consistent with those of the pristine carbonate samples (see Fig. 7, Table 1). Taking also into account the limited thickness of the P0 deposits exposed at Cerro Submarino, we considered all the collected samples as belonging to a single level and we calculated a unique $^{87}Sr/^{86}Sr$ age starting from five different samples.

Three shark teeth were chosen from the lower portion of the P0 sequence, a few meters above the PE0.0 unconformity, in the plain northward of Cerro Submarino, here informally called “Tooth plain” (see Fig. 3D). Of the analyzed teeth, Tooth 1 is a lower anterolateral tooth of *Cosmopolitodus hastalis*, Tooth 2 is an upper tooth of the same species (Fig. 4D), and Tooth 3 is a lower tooth of *Isurus oxyrinchus* (see Table 1). The three resulting $^{87}Sr/^{86}Sr$ values are slightly different from each other, but there are no morphological or chemical reasons to prefer one tooth over another and all these samples were selected for the final age calculation.

A few meters above the PE0.0 unconformity, a calcite nodule from within a baleen whale mandible (SUB-2, Table 1) was first selected following the hypothesis of precipitation during early diagenesis, similarly to what hypothesized for the dolomite nodules found inside bone cavities in the Pisco Formation (Gariboldi et al., 2015; Gioncada et al., 2016). However, SUB-2 has a very low $^{87}Sr/^{86}Sr$ value similar to the late diagenetic cements, suggesting a late diagenetic imprint of this nodule, and therefore it was discarded. Close to this sample, an oyster was collected (SUB-5, Fig. 3D), and the thin nacre layers were drilled, giving an $^{87}Sr/^{86}Sr$ value similar to those of the shark teeth. Finally, a few meters above, three samples were selected from level SUB-8bis (see Fig. 3D): one from the presumably pristine sheath of a barnacle (SUB-8bis1), one from the bulk sediment cemented inside the same barnacle shell (SUB-8bis2), and the last one from a completely recrystallized shell of a bivalve (SUB-8bis3) (Table 1). The samples from the bulk and the recrystallized bivalve indicate that, as in the Ct1 sequence, diagenesis resulted in a substantial reduction of the $^{87}Sr/^{86}Sr$ value and a consequent increase of the calculated ages. In turn, the pristine calcite of the barnacle sheath shows an $^{87}Sr/^{86}Sr$ value similar to the other pristine samples and was considered for the final age calculation.

Discarding samples affected by diagenesis, a mean $^{87}Sr/^{86}Sr$ value can be calculated starting from five samples collected from the lower part of the P0 sequence. Together, the three shark teeth, SUB-5, and SUB-8bis1 result in a mean age of 13.45 Ma, with an uncertainty time range spanning between 14.80 and 12.45 Ma. Consequently, by means of SIS, the P0 sequence can be placed in the Langhian–Serravallian (Table 2). The age of the P0 sequence is now resolved, but poorly constrained because of the scarcity of well-preserved specimens (allowing for just a few dated samples) and the intrinsic limits of the SIS method.

4.4. Thermophilic invertebrates and vertebrates from the P0 sequence

The thermophilic fossils identified from the P0 strata exposed in the vicinities of Cerro Submarino include both invertebrates and vertebrates (Fig. 8).

Among the invertebrates, three cypraeid inner molds could be identified as belonging to *Muracypraea ormenoi*, an extinct species that has been interpreted as a thermophilic taxon that likely shared the environmental and climatic preferences of extant *Muracypraea mus* (DeVries et al., 2006). Although the holotype of *M. ormenoi* was collected from Chilcatay beds, another specimen of the same species was reported by DeVries et al. (2006) from undifferentiated strata of the Pisco Formation in the vicinities of Cerro Submarino, where the P0 strata are mostly exposed (Di Celma et al., 2017, 2018a). Unfortunately, the poor preservation state of the inner molds observed by us does not allow an unambiguous identification of these cipraeid specimens at the genus and species levels (see Fig. 8A–C). A specimen of the gastropod *Ficus distans* was also found in these strata (personal communication by T.J. DeVries; Di Celma et al., 2017); according to DeVries and Frassinetti (2003) and Nielsen and Glodny (2009), *Ficus distans* should be regarded as a thermophilic member of a generally warm-water genus. Seven specimens belonging to the family Architectonicidae were also found (see Fig. 8H–J). Architectonicids were considered by Nielsen and Frassinetti (2007) as tropical and subtropical gastropods. Finally, the P0 invertebrate assemblage from the Cerro Submarino area includes the only known coral occurrence from the East Pisco Basin, reported in this paper for the first time. The single examined specimen consists of several tiny corallites (up to 4.5 mm in calicular diameter) settled on two large barnacle shells (Fig. 8F, G). The distal part of the corallites is badly preserved, however their size, shape, septal number, septal arrangement, and stolon-like connections allow us to ascribe the colony to the tropical to warm temperate family Rhizangidae (Cairns et al., 2005). Remarkable affinities with the genus *Culicia* have been noted, but further better preserved specimens are needed to confirm this genus-level identification.

With respect to the vertebrates, teeth and dermal spines belonging to several taxa of more or less thermophilic cartilaginous fishes have been collected from the studied P0 exposures. The elasmobranch assemblage includes abundant teeth of the requiem shark *Carcharhinus*, among which *Carcharhinus brachyurus* and *Carcharhinus* cf. *leucas* stand out. Most extant species of *Carcharhinus* are confined today to warm-temperate to tropical waters, and *C. leucas* is especially known as a tropical to sub-tropical species (Simpfendorfer and Burgess, 2009); in turn, *C. brachyurus* is a more temperate species that thrives in relatively cooler waters (Duffy and Gordon, 2003). Another carcharhinid genus, *Galeocerdo*, is known from the P0 by several teeth of the extinct species *Galeocerdo aduncus*, whose closest living relative (i.e., the tiger shark *Galeocerdo cuvier*) is known as a tropical/subtropical fish (Ferreira and Simpfendorfer, 2019); similar considerations also apply to the sole extant species of *Anoxypristis* (i.e., the knifetooth sawfish *Anoxypristis cuspidata*; D'Anastasi et al., 2013), a genus of rays represented in the lower Pisco strata by several rostral spines that cannot be determined at the species level. A predilection for tropical and warm-temperate waters is also regarded as characteristic of the extinct sharks *Carcharocles megalodon* (Purdy, 1996; Aguilera and Aguilera, 2004; but see also Pimiento et al., 2016, for a different interpretation) and *Hemipristis serra* (Fig. 8D, E); in particular, the extant snaggletooth shark *Hemipristis elongata* – the only living species of *Hemipristis* – is a tropical coastal shark that inhabits inshore and offshore waters up to 30 m depth (Compagno, 1984; Pimiento et al., 2016).

5. Discussion

5.1. SIS age of the P0 strata

Strontium data confirm a Burdigalian age for the Ct1 sequence of the Chilcatay Formation, in line with the ^{39}Ar–^{40}Ar dating on tephra and with the biostratigraphic results provided by diatoms and silicoflagellates from the localities of Roca Negra and Ullujaya (Belia and Nick, 2016; Di Celma et al., 2018b; Lambert et al., 2018; Bosio et al., 2019b). These SIS ages are in agreement with the older age of 19.25 ± 0.05 Ma of the PN-T2 ash layer dated by Bosio et al., 2019b at the base of the Chilcatay Formation at Roca Negra, and with the ages of 19.00 ± 0.28 Ma and 18.02 ± 0.07 Ma obtained from ash layers at the base and at the top of the Ullujaya succession (UJA-T35 and SOT-T3, respectively, of Bosio et al., 2019b; Di Celma et al., 2018b). In addition, they are consistent in themselves, with stratigraphically lower beds yielding older or at least matching ages, although this observation is limited by the broadly overlapping error ranges for each layer. Overall, the consistency of the strontium ages from the Ct1 sequence confirms the suitability of the method for dating sediments in the East Pisco Basin.

Our results also provide the first direct evidence for the age of the P0 sequence of the Pisco Formation in the study area, placing this unit in the middle Miocene (Langhian–Serravallian). This estimate is again consistent with the broad age constraints (ca. 18.0–9.5 Ma) imposed by previous radiometric dating and biostratigraphy (Di Celma et al., 2018b; Bosio et al., 2019b).

Current knowledge about both invertebrate and vertebrate assemblages of the P0 sequence is poorly informative in terms of chronostratigraphy; that said, a middle Miocene age matches the general aspect of the P0 oryctocoenosis. Indeed, mollusks suggest similarities with the lower–middle Miocene Navidad Formation of central Chile (DeVries and Frassinetti, 2003). Likewise, the baleen whale assemblage appears remarkably more archaic than that of the overlying P1 and P2 sequences (Di Celma et al., 2017; Marx et al., 2017b), with the presence of *Pelocetus* sp. (Bianucci et al., 2019) matching other early–middle Miocene occurrences of this genus from Japan (Kimura et al., 2007) and eastern North America (Kellogg, 1965). The occurrence of the archaic cetotheriid *Tiucetus rosae*, one of the earliest branching member of a mysticete family (i.e., Cetotheriidae) that flourished in late Miocene times (Marx et al., 2019b), also characterizes the P0 oryctocoenosis, possibly hinting at a middle Miocene age. Also notable is the abrupt increase in baleen whale abundance relative to the underlying Chilcatay Formation, which appears to reflect a global early–middle Miocene pattern (Bianucci et al., 2018; Marx et al., 2019a). Sharks and rays are of limited utility, as all the taxa recognized so far exhibit a stratigraphic range which spans for most of the Miocene at least. As a consequence, all the elasmobranch taxa recognized from the P0 sequence but *Carcharocles megalodon* and *Hemipristis serra,* are known from both the lower Miocene Chilcatay strata exposed in the Ullujaya-Zamaca areas (Bianucci et al., 2018; Di Celma et al., 2018b, 2019; Landini et al., 2019) and the upper Miocene Pisco strata (P1 and P2 sequences) exposed at Cerro Colorado (Di Celma et al., 2017; Landini et al., 2017a, Landini et al., 2017). *Carcharocles megalodon*, whose fossil record starts with the Burdigalian (Carrillo-Briceño et al., 2015; but see also Perez et al., 2018 in this regard), is well-known from the P1 and P2 beds but absent from the Chilcatay Formation, where the genus *Carcharocles* is represented by the more archaic species *Carcharocles chubutensis*. Conversely, *Hemipristis serra* is present in the Burdigalian deposits of the Chilcatay Formation, whereas it is absent from the younger P1 and P2 sequences, although it is known from outside the East Pisco Basin in deposits as young as the early Pleistocene (e.g., Ebersole et al., 2017).

5.2. Paleoclimatic significance of the P0 fossil assemblage

Previous investigations on the invertebrate assemblages from the P0 and P1 sequences revealed a marked faunal change coincident with the PE0.1 unconformity (Di Celma et al., 2017). Specifically, species such as *Ficus distans* and *Miltha* cf. *vidali*, which also occur in the Chilcatay Formation, associate P0 with the Navidad Formation of Chile, rather than the Panamic fauna (DeVries, 2002, 2007; DeVries and Frassinetti,

2003). According to Nielsen and Glodny (2009), an interpretation of the mollusk assemblage from the Navidad Formation in the light of the ecological preference of extant genera suggests water temperatures of at least 20 °C for the Navidad area (34°S) during the early-middle Miocene. Indeed, in the P0 sequence, the presence of warm-water or tropical taxa such as Architectonicidae and Cypraeidae (DeVries and Frassinetti, 2003; Nielsen and Frassinetti, 2007) (see Fig. 8A–C, H–J), as well as the occurrence of *Ficus*, indicates a warm-water, tropical paleoenvironment for this unit. This is also supported by the finding of the only coral colony ever collected from the East Pisco Basin, belonging to the family Rhizangiidae (Fig. 8F and G). Rhizangiid scleractinians are the most common corals in shallow-water tropical and warm temperate environments of the eastern Pacific; in particular, the P0 specimens appear as morphologically close to the Miocene to Holocene genus *Culicia*, which currently lives in the tropical and subtropical waters of the Indo-Pacific region (Cairns et al., 2005). On the whole, these observations support the paleoclimatic reconstruction proposed by DeVries and Frassinetti (2003), who hypothesized warm-water conditions for the southern Peruvian coast during the early and middle Miocene, in contrast with the cooler conditions during the late Miocene and early Pliocene.

Our data on the composition of the vertebrate oryctocoenosis from P0 further suggest tropical to subtropical thermal affinities for the paleoenvironment. In particular, among the recognized taxa, the knifetooth sawfish *Anoxypristis* is currently known as a nectobenthic organism that inhabits coastal and estuarine warm-water environments (e.g., D'Anastasi et al., 2013). Similarly, the extinct snaggletooth shark *Hemipristis serra* (Fig. 8D and E) is one of the most common chondrichthyan taxa in low-latitude neritic deposits of the Neogene, and its closest extant relative (*Hemipristis elongata*) is known as a tropical shallow-water shark (e.g., Compagno, 1984). Interestingly, there are no late Miocene occurrences of *H. serra* from the East Pisco Basin, even though this species persisted till the early Pleistocene in many tropical/subtropical chondrichthyan assemblages worldwide, and has even been recorded from the late Miocene strata of the Miramar Formation of northern Peru (Apolín et al., 2004).

It should be noted that the deposition of the P0 strata likely took place during the last phases of the Middle Miocene Climatic Optimum (= MMCO, the last major warming interval of the Cenozoic, occurred between 17 and 14 Ma; Loughney et al., 2019, and references therein) or the onset of the Middle Miocene Climatic Transition (= MMCT, the subsequent interval of gradual change towards cooler climatic conditions), i.e., during a period of globally high temperatures relative to the modern. As reported above, the warm, tropical paleoenvironment here reconstructed for the P0 sequence sets it apart from the remainder of the Pisco Formation, which is thought to reflect a cooler setting (e.g., Dunbar et al., 1990; DeVries and Frassinetti, 2003; Amiot et al., 2008; Di Celma et al., 2017). In particular, oxygen-isotope analyses on phosphatic remains of marine vertebrates from upper Miocene horizons of the Pisco Formation exposed in the Ica Desert (i.e., the CLB vertebrate level of Muizon and DeVries, 1985; referred to the late Miocene according to Di Celma et al., 2017) and the Sacaco area (i.e., the ELJ, AGL, SAS and SAO vertebrate levels of Muizon and DeVries, 1985; late Miocene in age according to Ehret et al., 2012) have revealed marine paleotemperatures that, on the whole, match those observed today off the coasts of Peru (Amiot et al., 2008). Overall, this pattern is suggestive of relatively cool conditions along the Peruvian coast during the late Miocene, which could be regarded as reflecting the post-MMCO trend of global cooling that culminated with ocean temperatures dipping to near-modern values around 7 and 5.4 Ma (Herbert et al., 2016). Furthermore, since the upper Miocene deposits of the Pisco Formation contain abundant diatomaceous siltstones that indicate the existence of high primary productivity resulting from strong and persistent coastal upwelling conditions (Dunbar et al., 1990; DeVries and Frassinetti, 2003; Di Celma et al., 2017), it is reasonable to hypothesize that the above pattern is also representative of a major regional oceanographic change – i.e., a middle or early late Miocene strengthening of the Humboldt Current (see also conclusion in Amiot et al., 2008). This change might also explain the local disappearance of *H. serra*, whose range likely contracted northwards as colder conditions took hold along the coasts of southern Peru.

6. Conclusions

Along the western side of the Ica River (Peru), the age of deposition of the P0 sequence, the lowest stratigraphic unit of the Pisco Formation, was an uncertain and debated issue. In the present study, Strontium Isotope Stratigraphy was applied on carbonates and phosphates of both the Chilcatay and Pisco formations for resolving the age of this paleontologically significant unit.

In this work, we provide new Burdigalian ages (18.8–18.0 Ma) for the Ct1 sequence of the Chilcatay Formation and propose a Langhian–Serravallian age (14.8–12.4 Ma) for the P0 sequence of the Pisco Formation (see Fig. 9). This estimate is consistent with the

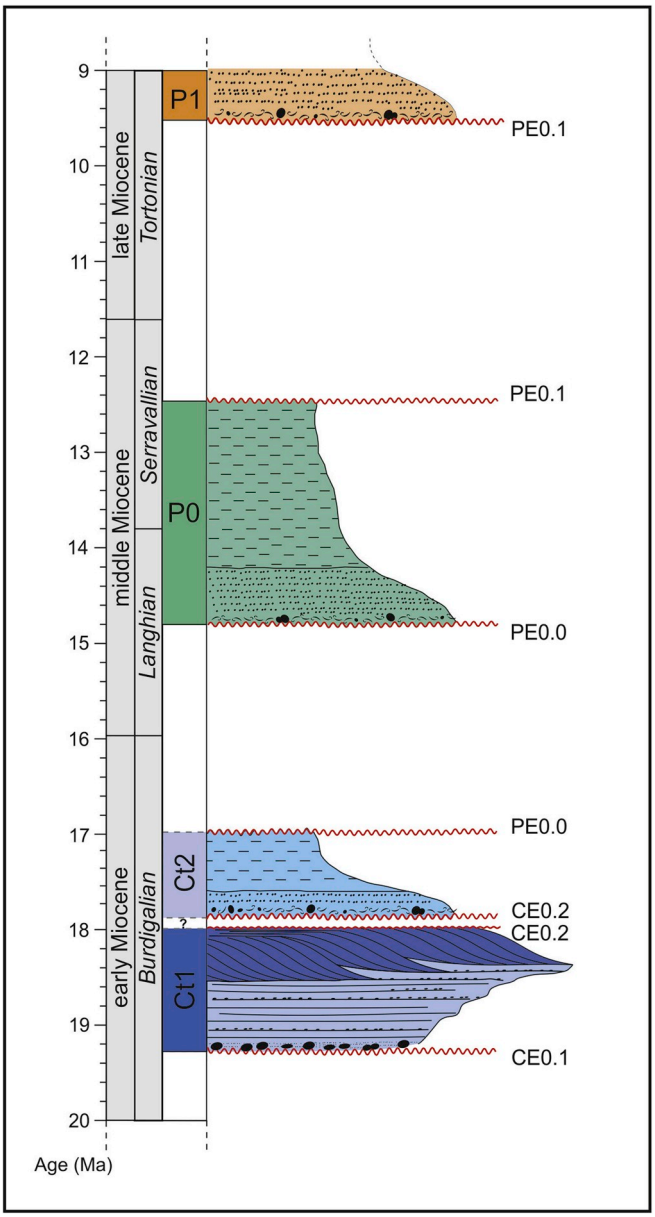

Fig. 9. Schematic chronostratigraphic section of the Chilcatay (Ct1 and Ct2) and Pisco (P0 and P1) sequences according to Strontium Isotope Stratigraphy.

relatively archaic aspect of the fossil assemblage from the lower Pisco strata, and provides a time constraint for a marked faunal change occurring across the PE0.1 unconformity. With respect to the Chilcatay Formation, the obtained Sr ages perfectly agree with previous ^{39}Ar–^{40}Ar ages on tephra layers and biostratigraphic results, confirming the feasibility of SIS in the studied deposits. This gives further reliability to the middle Miocene ages obtained by means of Sr isotope analyses for the P0 sequence.

Not least, both the invertebrate and vertebrate fossil assemblages indicate that the P0 sequence was deposited in a warm-water environment resembling that of the underlying Chilcatay Formation rather than the cooler and more productive setting of the overlying P1 and P2 sequences. We suggest that the marked cooling distinguishing P0 from the remainder of the Pisco Formation may reflect both the late Miocene trend of global cooling and a middle–late Miocene strengthening of the Humboldt Current.

Funding

This study was supported by grants from the Italian Ministero dell'Istruzione dell'Università e della Ricerca (PRIN Project, 2012YJSBMK) to G. Bi.; from the Università degli Studi di Milano-Bicocca to E.M. (2017-ATE-0466); from the Università di Pisa to G. Bi. (PRA_2017_0032); and an EU Marie Skłodowska-Curie Global Postdoctoral fellowship (656010/MYSTICETI) and an Australian Research Council DECRA fellowship (DE190101052) to F.G.M.

Acknowledgments

The authors are grateful to T.J. DeVries for information and helpful discussions on the age and paleoenvironment of the Pisco Formation. Special thanks to W. Landini, O. Lambert and C. de Muizon for interesting discussions on the vertebrate fauna, and to D. Basso and G. Coletti for helpful discussions on mollusk systematics and strontium dating. The authors would like to thank also R. Varas-Malca and W. Aguirre for assistance in the field, and D. Buhl for running the ICP-OES and Sr isotope analyses at Bochum University. The authors wish to thank F. Núñez for his valuable reviewing effort, and J. McArthur for the helpful criticism and for sharing the LOWESS 5 Table. Editorial support by Michelangelo Martini is also much appreciated.

Appendix A. Supplementary data

Supplementary data to this article can be found online at https://doi.org/10.1016/j.jsames.2019.102399.

References

Aguilera, O.A., Aguilera, D.R., 2004. Giant-toothed white sharks and wide-toothed mako (Lamnidae) from the Venezuela Neogene: their role in the Caribbean, shallow-water fish assemblage. Caribb. J. Sci. 40, 368–382.

Amiot, R., Göhlich, U.B., Lécuyer, C., Muizon, C. de, Cappetta, H., Fourel, F., Héran, M.-A., Martineau, F., 2008. Oxygen isotope compositions of phosphate from Middle Miocene–Early Pliocene marine vertebrates of Peru. Palaeogeogr. Palaeoclimatol. Palaeoecol. 264, 85–92.

Apolín, J., González, G., Martínez, J.M., 2004. Seláceos del Mioceno Superior de Quebrada Pajaritos (Piura, Perú). Actas XII Congreso Peruano de Geología. Sociedad Geológica del Perú, Perú, pp. 401–404.

Barbin, V., Ramseyer, K., Debenay, J.P., Schein, E., Roux, M., Decrouez, D., 1991. Cathodoluminescence of recent biogenic carbonates: an environmental and ontogenetic fingerprint. Geol. Mag. 128, 19–26.

Barbin, V., 2013. Application of cathodoluminescence microscopy to recent and past biological materials: a decade of progress. Mineral. Petrol. 107, 353–362.

Becker, A.M., Seidemann, D.E., Chamberlain Jr., J.A., Buhl, D., Slattery, W., 2008. Strontium isotopic signatures in the enameloid and dentine of upper Cretaceous shark teeth from western Alabama: paleoecologic and geochronologic implications. Palaeogeogr. Palaeoclimatol. Palaeoecol. 264, 188–194.

Belia, E.R., Nick, K.E., 2016. Early-Miocene calcareous nannofossil biostratigraphy from low-latitude, Pisco Basin, Peru. Geol. Soc. Am. Abstr. Progr. 48, 4.

Belia, E.R., Nick, K.E., Bedoya Agudelo, E., Watkins, D.K., 2019. Earliest Miocene calcareous nannofossil biostratigraphy from the low-latitude Pisco Basin (Peru). Stratigraphy 16, 87–105.

Bianucci, G., Collareta, A., Bosio, G., Landini, W., Gariboldi, K., Gioncada, A., Lambert, O., Malinverno, E., de Muizon, C., Varas-Malca, R., Villa, I.M., Coletti, G., Urbina, M., Di Celma, C., 2018. Taphonomy and palaeoecology of the lower Miocene marine vertebrate assemblage of Ullujaya (Chilcatay Formation, East Pisco basin, southern Peru). Palaeogeogr. Palaeoclimatol. Palaeoecol. 511, 256–279.

Bianucci, G., Di Celma, C., Collareta, A., Landini, W., Post, K., Tinelli, C., de Muizon, C., Bosio, G., Gariboldi, K., Gioncada, A., Malinverno, E., Cantalamessa, G., Altamirano-Sierra, A., Salas-Gismondi, R., Urbina, M., Lambert, O., 2016a. Fossil marine vertebrates of Cerro Los Quesos: distribution of cetaceans, seals, crocodiles, seabirds, sharks, and bony fish in a late Miocene locality of the Pisco Basin, Peru. J. Maps 12, 1037–1046.

Bianucci, G., Urbina, M., Lambert, O., 2015. A new record of *Notocetus vanbenedeni* (Squalodelphinidae, Odontoceti, Cetacea) from the early Miocene of Peru. Comptes Rendus Palevol 14, 5–13.

Bianucci, G., Bosio, G., Malinverno, E., de Muizon, C., Villa, I.M., Urbina, M., Lambert, O., 2018a. A new large squalodelphinid (Cetacea, Odontoceti) from Peru sheds light on the Early Miocene platanistoid disparity and ecology. Royal Soc. Open Sci. 5, 172302.

Bianucci, G., Di Celma, C., Landini, W., Post, K., Tinelli, C., de Muizon, C., Gariboldi, K., Malinverno, E., Cantalamessa, G., Gioncada, A., Collareta, A., Salas-Gismondi, R., Varas-Malca, R.M., Urbina, M., Lambert, O., 2016. Distribution of fossil marine vertebrates in Cerro Colorado, the type locality of the giant raptorial sperm whale *Livyatan melvillei* (Miocene, Pisco Formation, Peru). J. Maps 12, 543–557.

Bianucci, G., Di Celma, C., Urbina, M., Lambert, O., 2016. New beaked whales from the late Miocene of Peru and evidence for convergent evolution in stem and crown Ziphiidae (Cetacea, Odontoceti). PeerJ 4, e2479.

Bianucci, G., Marx, F.G., Collareta, A., Di Stefano, A., Landini, W., Morigi, C., Varola, A., 2019. Rise of the titans: baleen whales became giants earlier than thought. Biol. Lett. 15, 20190175.

Bosio, G., Gioncada, A., Malinverno, E., Di Celma, C., Villa, I.M., Cataldi, G., Gariboldi, K., Collareta, A., Urbina, M., Bianucci, G., 2019a. Chemical and petrographic fingerprinting of volcanic ashes as a tool for high-resolution stratigraphy of the upper Miocene Pisco Formation (Peru). J. Geol. Soc. 176, 13–28.

Bosio, G., Malinverno, E., Villa, I.M., Di Celma, C., Gariboldi, K., Gioncada, A., Barberini, B., Urbina, M., Bianucci, G. (in press). Tephrochronology and chronostratigraphy of the Miocene Chilcatay and Pisco formations (East Pisco Basin, Peru). Newsletter on Stratigraphy, DOI: 10.1127/nos/2019/0525.

Brand, L.R., Esperante, R., Chadwick, A.V., Porras, O.P., Alomía, M., 2004. Fossil whale preservation implies high diatom accumulation rate in the Miocene–Pliocene Pisco Formation of Peru. Geology 32, 165–168.

Brand, U., 1991. Strontium isotope diagenesis of biogenic aragonite and low-Mg calcite. Geochem. Cosmochim. Acta 55, 505–513.

Brand, U., Jiang, G., Azmy, K., Bishop, J., Montanez, I.P., 2012. Diagenetic evaluation of a Pennsylvanian carbonate succession (Bird Spring Formation, Arrow Canyon, Nevada, U.S.A.) — 1: Brachiopod and whole rock comparison. Chem. Geol. 308/309, 26–39.

Brand, U., Veizer, J., 1980. Chemical Diagenesis of a Multicomponent Carbonate System -1: Trace Elements. J. Sediment. Res. 50, 1219–1236.

Cairns, S.D., Häussermann, V., Försterra, G., 2005. A review of the Scleractinia (Cnidaria: Anthozoa) of Chile, with the description of two new species. Zootaxa 1018, 15–46.

Carrillo-Briceño, J.D., Maxwell, E., Aguilera, O.A., Sánchez, R., Sánchez-Villagra, M.R., 2015. Sawfishes and other elasmobranch assemblages from the Mio-Pliocene of the South Caribbean (Urumaco Sequence, Northwestern Venezuela). PLoS One 10 article #e0139230.

Coletti, G., Bosio, G., Collareta, A., Buckeridge, J., Consani, S., El Kateb, A., 2018. Palaeoenvironmental analysis of the Miocene barnacle facies: case studies from Europe and South America. Geol. Carpathica 69, 573–592.

Coletti, G., Bosio, G., Collareta, A., Malinverno, E., Bracchi, A.V., Di Celma, C., Basso, D., Stainbank, S., Spezzaferri, S., Cannings, T., Bianucci, G., 2019a. Biostratigraphic, evolutionary, and paleoenvironmental significance of the southernmost lepidocyclinids of the Pacific coast of South America (East Pisco Basin, southern Peru). J. South Am. Earth Sci. 96 article #102372.

Coletti, G., Collareta, A., Bosio, G., Buckeridge, J., Urbina M. (in press). Perumegabalanus calziai gen. et sp. nov., a new intertidal megabalanine barnacle from the early Miocene of Peru. Neues Jahrbuch fur Geologie und Palaontologie-Abhandlungen.

Collareta, A., Coletti, G., Bosio, G., Buckeridge, J., de Muizon, C., DeVries, T.J., Varas-Malca, R., Altamirano-Sierra, A., Urbina-Schmitt, M., Bianucci, G., 2019. A new barnacle (Cirripedia: Neobalanoformes) from the early Miocene of Peru: Palaeoecological and palaeobiogeographical implications. Neues Jahrb. Geol. Palaontol. Abh. 292, 321–338.

Collareta, A., Landini, W., Chalcatana, C., Valdivia, W., Altamirano-Sierra, A., Urbina-Schimtt, M., Bianucci, G., 2017. A well preserved skeleton of the fossil shark *Cosmopolitodus hastalis* from the late Miocene of Peru, featuring fish remains as fossilized stomach contents. Riv. Ital. Paleontol. Stratigr. 123, 11–22.

Collareta, A., Landini, W., Lambert, O., Post, K., Tinelli, C., Di Celma, C., Panetta, D., Tripodi, M., Salvadori, P.A., Caramella, D., Marchi, D., Urbina, M., Bianucci, G., 2015. Piscivory in a Miocene Cetotheriidae: first record of fossilized stomach content for an extinct baleen-bearing whale. Sci. Nat. 102 article #70.

Compagno, L.J.V., 1984. FAO Species Catalogue. Vol 4: Sharks of the world, Part 2 - Carcharhiniformes. FAO Fisheries 4 (2), 251–633 Synopsis No. 125.

Cox, L.R., Newell, N.D., Boyd, D.W., Branson, C.C., Casey, R., Chavan, A., Coogan, A.H., Dechaseaux, C., Fleming, C.A., Haas, F., Hertlein, L.G., Kauffman, E.G., Keen, A.M., Larocque, A., McAlester, A.L., Moore, R.C., Nuttall, C.P., Perkins, B.F., Purl, H.S., Smith, L.A., Soot-Ryen, T., Stenzel, H.B., Trueman, E.R., Turner, R.T., Weir, J., 1971. Part N. Mollusca (Bivalvia). In: Moore, R.C. (Ed.), Treatise of Invertebrate Paleontology. Lawrence, Meriden and New York. The University of Kansas Printing Service, pp. N1–N1224.

Crippa, G., Ye, F., Malinverno, C., Rizzi, A., 2016. Which is the best method to prepare invertebrate shells for SEM analysis? Testing different techniques on recent and fossil brachiopods. Boll. Soc. Paleontol. Ital. 55, 111–125.
DeVries, T.J., 2002. Patterns of diversity in Cenozoic marine mollusks from the Peruvian province. Geol. Soc. Am. Abstr. Progr. 34, 39.
DeVries, T.J., 2007. Molluscan evidence bearing on Cenozoic warm upwelling off southern Peru. Geol. Soc. Am. Abstr. Progr. 39, 78.
DeVries, T.J., Jud, N.A., 2018. Lithofacies patterns and paleogeography of the Miocene Chilcatay and lower Pisco depositional sequences (East Pisco Basin, Peru). Boletín de la Sociedad Geológica del Perú, Volumen Jubilar 8, 124–167.
D'Anastasi, B., Simpfendorfer, C., van Herwerden, L., 2013. *Anoxypristis cuspidata*. In: The IUCN Red List of Threatened Species 2013: e.T39389A18620409, . http://www.iucnredlist.org, Accessed date: 28 April 2018.
DeVries, T.J., 1998. Oligocene deposition and Cenozoic sequence boundaries in the Pisco Basin (Peru). J. South Am. Earth Sci. 11, 217–231.
DeVries, T.J., 2016. Fossil Cenozoic crassatelline bivalves from Peru: New species and generic insights. Acta Palaeontol. Pol. 61, 661–688.
DeVries, T.J., 2017. Eocene Stratigraphy and Depositional History near Puerto Caballas (East Pisco Basin, Peru). Boletín de la Sociedad Geológica del Perú 112, 39–52.
DeVries, T.J., Frassinetti, D., 2003. Range extensions and biogeographic implications of Chilean Neogene mollusks found in Peru. Boletín del Museo Nacional de Historia Natural, Chile 52, 119–135.
DeVries, T.J., Groves, L.T., Urbina, M., 2006. A new early miocene Muracypraea Woodring, 1957 (Gastropoda: Cypraeidae) from the Pisco Basin of southern Peru. Nautilus 120, 101–105.
DeVries, T.J., Schrader, H., 1997. Middle Miocene marine sediments in the Pisco Basin (Peru). Bol. Soc. Geol. Peru 87, 1–13.
DeVries, T.J., Urbina, M., Jud, N.A., 2017. The Eocene-Oligocene Otuma Depositional Sequence (East Pisco Basin, Peru): Paleogeographic and Paleoceanographic Implications of New Data. Boletín de la Sociedad Geológica del Perú 112, 14–38.
Di Celma, C., Malinverno, E., Bosio, G., Collareta, A., Gariboldi, K., Gioncada, A., Molli, G., Basso, D., Varas-Malca, R.M., Pierantoni, P.P., Villa, I.M., Lambert, O., Landini, W., Sarti, G., Cantalamessa, G., Urbina, M., Bianucci, G., 2017. Sequence stratigraphy and paleontology of the upper Miocene Pisco Formation along the western side of the lower Ica valley (Ica Desert, Peru). Riv. Ital. Paleontol. Stratigr. 123, 255–274.
Di Celma, C., Malinverno, E., Bosio, G., Gariboldi, K., Collareta, A., Gioncada, A., Landini, W., Pierantoni, P.P., Bianucci, G., 2018a. Intraformational unconformities as a record of late Miocene eustatic falls of sea level in the Pisco Formation (southern Peru). J. Maps 14, 607–619.
Di Celma, C., Malinverno, E., Collareta, A., Bosio, G., Gariboldi, K., Lambert, O., Landini, W., Gioncada, A., Villa, I.M., Coletti, G., de Muizon, C., Urbina, M., Bianucci, G., 2018b. Facies analysis, stratigraphy and marine vertebrate assemblage of the early Miocene Chilcatay Formation at Ullujaya (Pisco basin, Peru). J. Maps 14, 257–268.
Di Celma, C., Pierantoni, P.P., Malinverno, E., Collareta, A., Lambert, O., Landini, W., Bosio, G., Gariboldi, K., Gioncada, A., de Muizon, C., Molli, G., Marx, F.G., Varas-Malca, R.M., Urbina, M., Bianucci, G., 2019. Allostratigraphy and paleontology of the lower Miocene Chilcatay Formation in the Zamaca area, East Pisco basin, southern Peru. J. Maps 15, 393–405.
Duffy, C., Gordon, I., 2003. *Carcharhinus brachyurus*. In: The IUCN Red List of Threatened Species 2003: e.T41741A10551730, . http://www.iucnredlist.org, Accessed date: 28 April 2018.
Dunbar, R.B., Marty, R.C., Baker, P.A., 1990. Cenozoic marine sedimentation in the Sechura and Pisco basins, Peru. Palaeogeogr. Palaeoclimatol. Palaeoecol. 77, 235–261.
Ebersole, J.A., Ebersole, S.M., Cicimurri, D.J., 2017. The occurrence of early Pleistocene marine fish remains from the Gulf Coast of Mobile County, Alabama, USA. Palaeodiversity 10, 97–116.
Ehret, D.J., MacDaffen, B.J., Jones, D.S., DeVries, T.J., Foster, D.A., Salas-Gismondi, R., 2012. Origin of the white shark Carcharodon (Lamniformes: Lamnidae) based on recalibration of the upper Neogene Pisco Formation of Peru. Palaeontology 55, 1139–1153.
Enax, J., Janus, A.M., Raabe, D., Epple, M., Fabritius, H.O., 2014. Ultrastructural organization and micromechanical properties of shark tooth enameloid. Acta Biomater. 10, 3959–3968.
Esperante, R., Brand, L., Nick, K.E., Poma, O., Urbina, M., 2008. Exceptional occurrence of fossil baleen in shallow marine sediments of the Neogene Pisco Formation, Southern Peru. Palaeogeogr. Palaeoclimatol. Palaeoecol. 257, 344–360.
Faure, G., Mensing, T.M., 2005. Isotopes: Principles and Applications. John Wiley & Sons, New York.
Ferreira, L.C., Simpfendorfer, C., 2019. *Galeocerdo cuvier*. In: The IUCN Red List of Threatened Species 2019:e.T39378A291354, . http://www.iucnredlist.org, Accessed date: 25 March 2019.
Frijia, G., Parente, M., 2008. Strontium isotope stratigraphy in the upper Cenomanian shallow-water carbonates of the southern Apennines: Short-term perturbations of marine $^{87}Sr/^{86}Sr$ during the oceanic anoxic event 2. Palaeogeogr. Palaeoclimatol. Palaeoecol. 261, 15–29.
Frijia, G., Parente, M., Di Lucia, M., Mutti, M., 2015. Carbon and strontium isotope stratigraphy of the Upper Cretaceous (Cenomanian-Campanian) shallow-water carbonates of southern Italy: Chronostratigraphic calibration of larger foraminifera biostratigraphy. Cretac. Res. 53, 110–139.
Gariboldi, K., Bosio, G., Malinverno, E., Gioncada, A., Di Celma, C., Villa, I.M., Urbina, M., Bianucci, G., 2017. Biostratigraphy, geochronology and sedimentation rates of the upper Miocene Pisco Formation at two important marine vertebrate fossil-bearing sites of southern Peru. Newsl. Stratigr. 50, 417–444.
Gariboldi, K., Gioncada, A., Bosio, G., Malinverno, E., Di Celma, C., Tinelli, C., Cantalamessa, G., Landini, W., Urbina, M., Bianucci, G., 2015. The dolomite nodules enclosing fossil marine vertebrates in the East Pisco Basin, Peru: field and petrographic insights into the Lagerstätte formation. Palaeogeogr. Palaeoclimatol. Palaeoecol. 438, 81–95.
Gioncada, A., Collareta, A., Gariboldi, K., Lambert, O., Di Celma, C., Bonaccorsi, E., Urbina, M., Bianucci, G., 2016. Inside baleen: exceptional microstructure preservation in a late Miocene whale skeleton from Peru. Geology 44, 839–842.
Gioncada, A., Gariboldi, K., Collareta, A., Di Celma, C., Bosio, G., Malinverno, E., Lambert, O., Pike, J., Urbina, M., Bianucci, G., 2018a. Looking for the key to preservation of fossil marine vertebrates in the Pisco Formation of Peru: new insights from a small dolphin skeleton. Andean Geol. 45, 379–398.
Gioncada, A., Petrini, R., Bosio, G., Gariboldi, K., Collareta, A., Malinverno, E., Bonaccorsi, E., Di Celma, C., Pasero, M., Urbina, M., Bianucci, G., 2018b. Insights into the diagenetic environment of fossil marine vertebrates of the Pisco Formation (late Miocene, Peru) from mineralogical and Sr-isotope data. J. South Am. Earth Sci. 81, 141–152.
Hampel, A., 2002. The migration history of the Nazca Ridge along the Peruvian active margin: A re-evaluation and some geological implications. Earth Planet. Sci. Lett. 203, 665–679.
Harrel Jr., T.L., Pérez-Huerta, A., Phillips, G., 2016. Strontium isotope age-dating of fossil shark tooth enameloid from theUpper Cretaceous Strata of Alabama and Mississippi, USA. Cretac. Res. 62, 1–12.
Herbert, T.D., Lawrence, K.T., Tzanova, A., Peterson, L.C., Caballero-Gill, R., Kelly, C.S., 2016. Late Miocene global cooling and the rise of modern ecosystems. Nat. Geosci. 9, 843.
Hsu, J.T., 1992. Quaternary uplift of the Peruvian coast related to the subduction of the Nazca Ridge: 13.5 to 15.6 degrees South latitude. Quat. Int. 15/16, 87–97.
Kellogg, R., 1965. Fossil marine mammals from the Miocene Calvert Formation of Maryland and Virginia, part 1: a new whalebone whale from the Miocene Calvert Formation. US. Nat. Museum Bull. 247, 1–45.
Kimura, T., Hasegawa, Y., Ohzawa, H., Yamaoka, T., Furukawa, Y., Ueda, T., Kiyoshi, T., Sugihara, M., Sakuda, M., 2007. A mysticete whale (Cetacea) skeleton from the middle Miocene Bihoku Group, Shobara, Hiroshima, Japan. Misc. Rep. Hiwa Mus. Nat. Hist. 48, 1–10.
Kulm, L.D., Resig, J.M., Thornburg, T.M., Schrader, H.J., 1982. Cenozoic structure, stratigraphy and tectonics of the central Peru forearc. In: Legget, J.K. (Ed.), Trench and Forearc Geology: Sedimentation and Tectonics on Modern and Ancient Plate Margins. Blackwells, London, pp. 151–169.
Lambert, O., Bianucci, G., de Muizon, C., 2017a. Macroraptorial sperm whales (Cetacea, Odontoceti, Physeteroidea) from the Miocene of Peru. Zool. J. Linn. Soc. 179, 404–474.
Lambert, O., Bianucci, G., Urbina, M., 2014. *Huaridelphis raimondii*, a new early Miocene Squalodelphinidae (Cetacea, odontoceti) from the Chilcatay Formation, Peru. J. Vertebr. Paleontol. 34, 987–1004.
Lambert, O., Bianucci, G., Urbina, M., Geisler, J.H., 2017b. A new inioid (Cetacea, Odontoceti, Delphinidae) from the Miocene of Peru and the origin of modern dolphin and porpoise families. Zool. J. Linn. Soc. 179, 919–946.
Lambert, O., Collareta, A., Landini, W., Post, K., Ramassamy, B., Di Celma, C., Urbina, M., Bianucci, G., 2015a. No deep diving: evidence of predation on epipelagic fish for a stem beaked whale from the Late Miocene of Peru. Proc. R. Soc. Biol. Sci. 282 article #20151530.
Lambert, O., de Muizon, C., Bianucci, G., 2015b. A new archaic homodont toothed cetacean (Mammalia, Cetacea, Odontoceti) from the early Miocene of Peru. Geodiversitas 37, 79–108.
Lambert, O., de Muizon, C., Malinverno, E., Di Celma, C., Urbina, M., Bianucci, G., 2018. A new odontocete (toothed cetacean) from the Early Miocene of Peru expands the morphological disparity of extinct heterodont dolphins. J. Syst. Palaeontol. 16, 981–1016.
Landini, W., Altamirano-Sierra, A., Collareta, A., Di Celma, C., Urbina, M., Bianucci, G., 2017a. The late Miocene elasmobranch assemblage from Cerro Colorado (Pisco Formation, Peru). J. South Am. Earth Sci. 73, 168–190.
Landini, W., Collareta, A., Di Celma, C., Malinverno, E., Urbina, M., Bianucci, G., 2019. The early Miocene elasmobranch assemblage from Zamaca (Chilcatay Formation, Peru). J. South Am. Earth Sci. 91, 352–371.
Landini, W., Collareta, A., Pesci, F., Di Celma, C., Urbina, M., Bianucci, G., 2017. A secondary nursery area for the copper shark *Carcharhinus brachyurus* from the late Miocene of Peru. J. South Am. Earth Sci. 78, 164–174.
León, W., Aleman, A., Torres, V., Rosell, W., De la Cruz, O., 2008. Estratigrafía, sedimentología y evolución tectónica de la cuenca Pisco Oriental. Boletín INGEMMET 27, 144.
Loughney, K.M., Hren, M.T., Smith, S.Y., Pappas, J.L., 2019. Vegetation and Habitat Change in Southern California through the Middle Miocene Climatic Optimum: Paleoenvironmental Records from the Barstow Formation. Geological Society of America Bulletin, Mojave Desert, USA.
Macharé, J., Ortlieb, L., 1992. Plio-Quaternary vertical motions and the subduction of the Nazca Ridge, central coast of Peru. Tectonophysics 205, 97–108.
Marocco, R., de Muizon, C., 1988. Le Bassin Pisco, bassin cénozoïque d'avant arc de la côte du Pérou central: analyse géodynamique de son remplissage. Geodynamique 3, 3–19.
Marx, F.G., Collareta, A., Gioncada, A., Post, K., Lambert, O., Bonaccorsi, E., Urbina, M., Bianucci, G., 2017a. How whales used to filter: exceptionally preserved baleen in a Miocene cetotheriid. J. Anat. 231, 212–220.
Marx, F.G., Fitzgerald, E.M., Fordyce, R.E., 2019a. Like phoenix from the ashes: How modern baleen whales arose from a fossil "dark age". Acta Palaeontol. Pol. 64, 231–238.
Marx, F.G., Lambert, O., de Muizon, C., 2017b. A new Miocene baleen whale from Peru deciphers the dawn of cetotheriids. Royal Soc. Open Sci. 4 article #170560.

Marx, F.G., Post, K., Bosselaers, M., Munsterman, D.K., 2019b. A large Late Miocene cetotheriid (Cetacea, Mysticeti) from the Netherlands clarifies the status of Tranatocetidae. PeerJ 7 article #e6426.
McArthur, J., 1994. Recent Trends in Strontium Isotope Stratigraphy. Terra. Nova 6, 331–358.
McArthur, J.M., Howarth, R.J., Shields, G.A., 2012. Strontium Isotope Stratigraphy. In: Gradstein, F.M., Ogg, J.G., Schmitz, M., Ogg, G. (Eds.), The Geologic Time Scale 2012. Elsevier, Oxford, pp. 127–144.
Muizon, C. de, DeVries, T.J., 1985. Geology and paleontology of late Cenozoic marine deposits in the Sacaco area (Peru). Geol. Rundsch. 74, 547–563.
Nielsen, S.N., Frassinetti, D., 2007. The Miocene Architectonicidae (Gastropoda) of Chile. Paläontol. Z. 81/3, 291–303.
Nielsen, S.N., Glodny, J., 2009. Early Miocene subtropical water temperatures in the southeast Pacific. Palaeogeogr. Palaeoclimatol. Palaeoecol. 280, 480–488.
North American Commission on Stratigraphic Nomenclature [NACSN], 2005. North American stratigraphic code. AAPG (Am. Assoc. Pet. Geol.) Bull. 89, 1547–1591.
Penven, P., Echevin, V., Pasapera, J., Colas, F., Tam, J., 2005. Average circulation, seasonal cycle, and mesoscale dynamics of the Peru Current System: a modeling approach. J. Geophys. Res. 110, C10021.
Perez, V.J., Godfrey, S.J., Kent, B.W., Weems, R.E., Nance, J.R., 2018. The transition between *Carcharocles chubutensis* and *Carcharocles megalodon* (Otodontidae, Chondrichthyes): lateral cusplet loss through time. J. Vertebr. Paleontol. 38 article #e1546732.
Pilger, R.H., 1981. Plate reconstructions, aseismic ridges, and low-angle subduction beneath the Andes. Geol. Soc. Am. Bull. 92, 448–456.
Pimiento, C., MacFadden, B.J., Clements, C.F., Varela, S., Jaramillo, C., Velez-Juarbe, J., Silliman, B.R., 2016. Geographical distribution patterns of *Carcharocles megalodon* over time reveal clues about extinction mechanisms. J. Biogeogr. 43, 1645–1655.
Purdy, R.W., 1996. Paleoecology of fossil white sharks. In: Klimley, A.P., Ainley, D.G. (Eds.), Great White Sharks: the Biology of *Carcharodon carcharias*. Academic Press, San Diego, pp. 67–78.
Santos, A., Mayoral, E., Muñiz, F., 2005. Bioerosion scars of acorn barnacles from the southwestern Iberian Peninsula, upper Neogene. Rivista Itliana di Paleontologia e Stratigrafia 111, 181–189.
Scasso, R.A., McArthur, J.M., del Río, C.J., Martínez, S., Thirlwall, M.F., 2001. $^{87}Sr/^{86}Sr$ Late Miocene age of fossil molluscs in the “Entrerriense” of the Valdés Peninsula (Chubut, Argentina). J. South Am. Earth Sci. 14, 319–329.
Simpfendorfer, C.A., Burgess, G.H., 2009. *Carcharhinus leucas*. In: The IUCN Red List of Threatened Species 2013: e.T39372A10187195, . http://www.iucnredlist.org, Accessed date: 28 April 2018.
Steuber, T., 1999. Isotopic and chemical intra-shell variations in low-Mg calcite of rudist bivalves (Mollusca: Hippuritacea): disequilibrium fractionations and Late Cretaceous seasonality. Int. J. Earth Sci. 88, 551–570.
Steuber, T., 2003. Strontium isotope chemostratigraphy of rudist bivalves and cretaceous carbonate platforms. In: In: Gili, E., Negra, M.E.H., Skelton, P.W. (Eds.), North African Cretaceous Carbonate Platform Systems. NATO Science Series, IV, vol. 28. Earth and Environmental Sciences, pp. 229–238.
Thornburg, T.M., Kulm, L.D., 1981. Sedimentary basins of the Peru continental margin: structure, stratigraphy, and Cenozoic tectonics from 6°S to 16°S latitude. In: In: Kulm, L.D., Dymond, J., Dasch, E.J., Hussong, D.M. (Eds.), Nazca Plate: Crustal Formation and Andean Convergence, vol. 154. Geological Society of America Memoir, pp. 393–422.
Travis, R.B., Gonzales, G., Pardo, A., 1974. Hydrocarbon Potential of Coastal Basins of Peru. AAPG (Am. Assoc. Pet. Geol.) Bull. 58 1460-1460.
Ullmann, C.V., Korte, C., 2015. Diagenetic alteration in low-Mg calcite from macrofossils: a review. Geol. Q. 59, 3–20.
Zúñiga-Rivero, F.J., Klein, G.D., Hay-Roe, H., Álvarez-Calderon, E., 2010. The Hydrocarbon Potential of Peru. BPZ Exploración & Producción S.R.L, Lima.